

Chapter 3

The Lakshadweep High and Low

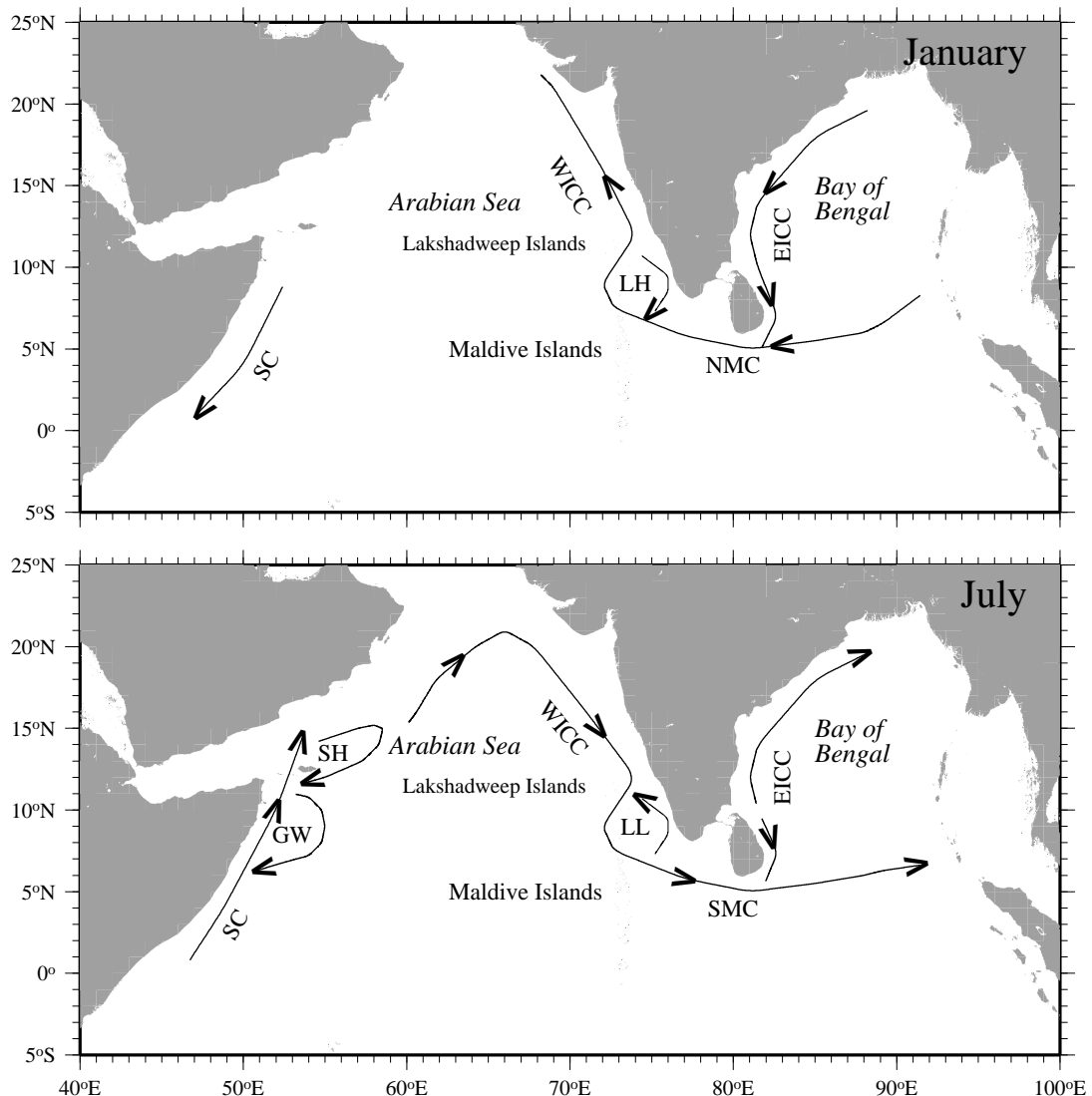
3.1 Observational Background

The monsoon winds that sweep across the north Indian Ocean force considerable seasonal changes in surface circulation. The most prominent and the best documented of these is seen off the coast of Somalia [Schott, 1986]. The Somali Current (Figure 3.1), which flows along the coast, is poleward during the southwest monsoon (June–September) and equatorward during the northeast monsoon (November–March). Other currents too, though not as energetic, reverse seasonally; for example, the Southwest Monsoon Current (SMC¹) and the Northeast Monsoon Current (NMC) south of Sri Lanka, the equatorial jet along the equator [Wyrтки, 1973], and the currents along the east and west coasts of India [Shetye et al., 1990, 1991a,b, 1993, 1996]. Associated with the changes in surface currents are variations in patterns of sea-surface topography, which appear, strengthen, and either decay or propagate away from the region of genesis year after year. The best studied amongst these is the Great Whirl, an anticyclonic gyre, with a high in surface topography, that forms between 5° and 10°N off Somalia with the onset of the southwest monsoon in June [Bruce, 1968]. It peaks during July–August and decays in September. The occurrence of another such high, though not as energetic, was discovered by Bruce et al. [1994]; using hydrographic data collected during the IIOE, they showed that a high forms off southwest India during the northeast monsoon. A low forms in the same region during the southwest monsoon (Figure 3.1). It was mentioned by Bruce [1968] and Bruce et al. [1994] and is seen in maps of geopotential topography [Wyrтки, 1971].

Though the occurrence of the high and low off southwest India was established using traditional hydrographic data, its annual cycle in relation to the annual cycle of sea-level perturbations in the rest of the Indian Ocean was appreciated better only after data from satellite altimetry

¹The Southwest Monsoon Current is often, perhaps usually, referred to as the Indian Monsoon Current (IMC). SMC appears to be a better acronym, given that its counterpart during the northeast monsoon is called NMC (Northeast Monsoon Current).

Figure 3.1 A schematic of the surface circulation in the north Indian Ocean during January and July. Abbreviations are as follows: LH, Lakshadweep high; LL: Lakshadweep low; GW, Great Whirl; SH, Socotra high; EICC, East India Coastal Current; WICC, West India Coastal Current; SC, Somali Current; NMC, Northeast Monsoon Current; and SMC, Southwest Monsoon Current. In January, the equatorward EICC and poleward WICC are connected by the NMC. In July, there is no apparent connection between the EICC, which flows poleward along the coast of India, and the equatorward WICC because the EICC is equatorward off Sri Lanka [Vinayachandran and Yamagata, 1998]. The WICC flows into the eastward SMC; the WICC in July is often considered part of the SMC because this is a continuous current flowing across the Arabian Sea into the Bay of Bengal. Consistency, however, requires that the current be called WICC when it flows along the west coast of India.



became available. Bruce et al. [1994] used Geosat altimetry to support inferences drawn from hydrography; Perigaud and Delecluse [1992] also used Geosat data to describe the annual cycle of sea level in the Indian Ocean.

The high and low off southwest India are seen in TOPEX/POSEIDON altimetry [Tapley et al., 1994; Nerem et al., 1994]. The altimeter data show that sea level starts rising off southwest India during December, when the East India Coastal Current (EICC²) is equatorward [Shetye et al., 1996]. The EICC flows into the NMC, which turns around the southern tip of Sri Lanka [Rao et al., 1989; Cutler and Swallow, 1984] and joins the poleward West India Coastal Current (WICC³) [Shetye et al., 1991a]. By early January, the positive anomalies of sea level spread offshore and northward along the west coast of India, and a circular high forms to the east of the Lakshadweep islands. By February, the high is no longer circular: it has stretched westward. By April, positive anomalies in sea level are seen all over the Arabian Sea. The evolution of the low proceeds in a similar fashion. First, sea level drops off southwest India in June, when the WICC is equatorward [Shetye et al., 1990]; the WICC turns around Sri Lanka and joins the eastward SMC. The EICC is poleward off the Indian coast at this time [Shetye et al., 1991b], but it is equatorward off Sri Lanka [Rao et al., 1989; Cutler and Swallow, 1984; McCreary et al., 1996; Vinayachandran and Yamagata, 1998]. Second, the negative anomalies spread offshore and along the coast, and a circular low forms to the east of the Lakshadweep islands during July–August. Third, the low stretches westward, and by the end of October, negative anomalies in sea level occur all over the Arabian Sea. This series of events is also seen in altimeter sea level for other years. These observations suggest that the formation of the high (low) off southwest India during the northeast (southwest) monsoon is one manifestation of an annual cycle of events that are linked not only to the coastal currents around India, but also to the circulation in the southern Arabian Sea as a whole.

3.2 Theoretical Background

A tropical ocean responds rapidly to a change in winds; Lighthill [1969] showed that the equatorial Rossby waves excited by the onset of the southwest monsoon reach the African coast in less than a month. The rest of the north Indian Ocean responds similarly to the monsoon winds: Rossby

²The EICC is the current along the east coast of India and Sri Lanka; the name remains the same irrespective of the season and the direction of the current. The EICC also flows along the east coast of Sri Lanka, and its direction along the Lankan coast is often different from that along the Indian coast farther north [McCreary et al., 1996; Vinayachandran and Yamagata, 1998].

³The WICC is the west-coast counterpart of the EICC; the name remains the same irrespective of the season and the direction of the current. The existence of the Lakshadweep high and low lead to the WICC being poleward over a part of the coast and equatorward over another part of the coast. There is some ambiguity about the name during the southwest monsoon; the equatorward WICC in July is often considered part of the SMC because this is a continuous current flowing across the Arabian Sea into the Bay of Bengal (Figure 3.1). Consistency, however, requires that the current be called WICC when it flows along the west coast of India.

waves and equatorial and coastal Kelvin waves have a profound effect on its dynamics, forcing changes not only locally in the region of generation, but also remotely. Investigations over the last decade have shown that these waves link the circulation in the Bay of Bengal, the Arabian Sea, and the equatorial Indian Ocean [Potemra et al., 1991; Yu et al., 1991; Perigaud and Delecluse, 1992; McCreary et al., 1993; Shankar et al., 1996; McCreary et al., 1996; Shankar and Shetye, 1997; Vinayachandran, 1995; Vinayachandran et al., 1996; Vinayachandran and Yamagata, 1998].

Yu et al. [1991] showed that an annual equatorial Kelvin wave, on reflection from the eastern boundary, propagates along the perimeter of the Bay of Bengal as a coastal Kelvin wave, radiating westward propagating Rossby waves in the process, and forces changes in the EICC. McCreary et al. [1993] showed that the winds along the eastern boundary of the bay also set up a similar Kelvin wave. They concluded that these Kelvin waves, besides contributing to the dynamics of the EICC [McCreary et al., 1996], bend around Sri Lanka to propagate along the Indian west coast, forcing changes in the WICC. Their simulations produce the high in January and the low in October. The idealized simulations of Yu et al. [1991] also produce the high and low, indicating an annual cycle. Bruce et al. [1994] noted that the high of Yu et al. appears to be a consequence of Rossby wave radiation by coastal Kelvin waves off southwest India. They also pointed out another possible mechanism for the high: a patch of anticyclonic wind-stress curl off the southern tip of India during the northeast monsoon. The wind-stress curl is cyclonic in this region during the southwest monsoon.

In the remainder of this chapter, we study the dynamics of the high and low, specifically addressing the following issues.

1. Many highs and lows that form in the world ocean, particularly those that have been described as eddies (the Gulf Stream eddies, the Great Whirl, etc.), are nonlinear in character. It is the nonlinearity in their dynamics that spins off these systems. Are the Lakshadweep high and low too of a similar kind?
2. How are they linked to the coastal currents off India? Are they forced primarily by winds local to the region, or is remote forcing significant?

Our primary tool in this study is a dynamical $1\frac{1}{2}$ -layer reduced-gravity model, which is the simplest realistic model of the surface circulation in the ocean. Experiments with both nonlinear and linear versions of the model indicate that nonlinearity in the momentum balance is not essential to simulate the high and the low, allowing us to simplify the problem. Simulations with a linear reduced-gravity model, shorn of the complexity inherent in the wind forcing, show that a Kelvin wave propagating along the Indian east coast can lead to the high and low. Then we simplify the dynamics further and obtain an analytic solution, showing that the dynamics of linear waves on an equatorial β -plane can simulate the high and low. This leads to a discussion on the forcing

mechanisms, where we examine the effects of local and remote forcing. We conclude the chapter with a discussion on the implications of the Lakshadweep high and low.

3.3 Numerical Simulation of the Lakshadweep High and Low

3.3.1 The Numerical Model

We use a dynamical $1\frac{1}{2}$ -layer reduced-gravity model to simulate the seasonal cycle of circulation in the southeastern Arabian Sea. The density of the model layers does not vary in space or time. The equations for the active upper layer⁴, are

$$(H\mathbf{v})_t + \nabla \cdot (\mathbf{v}H\mathbf{v}) + f\mathbf{k} \times (H\mathbf{v}) + g\bar{\Gamma}H\nabla H = \tau/\rho_1 + \nu\nabla^2(H\mathbf{v}) - \chi\mathbf{i} \cdot (H\mathbf{v}) \quad (3.1a)$$

$$H_t + \nabla \cdot (H\mathbf{v}) = \kappa\nabla^2 H \quad (3.1b)$$

$$\eta = \bar{\Gamma}(H - \bar{H}) \quad (3.1c)$$

where H is the instantaneous layer thickness, \bar{H} the initial layer thickness, $\mathbf{v} = (u, v)$ the velocity, $f = \beta y$ the Coriolis parameter, $\tau = (\tau^x, \tau^y)$ the wind stress, g the acceleration due to gravity, and $\bar{\Gamma} = \Delta\rho/\bar{\rho}$ the reduced-gravity parameter, with $\Delta\rho = \rho_2 - \rho_1$. $\bar{\rho}$ is an average density that is representative of the ocean. ν and κ are the Laplacian mixing coefficients for momentum and thickness, the latter being included to damp the small-scale noise in the H field, and χ is a Rayleigh friction coefficient. η is the deviation of model dynamic height, computed with respect to the motionless deep ocean, from the initial state. In the discussion that follows, we refer to η as the model sea level rather than as dynamic height. The model parameters are listed in Table 3.1.

Equations (3.1) are integrated numerically on a staggered Arakawa-C grid using the leapfrog scheme; diffusive terms are evaluated at the backward time level and all other terms at the central time level. To inhibit time-splitting instability, the fields are averaged between successive time levels every 41 time steps. The model domain, shown in Figure 3.2, is as in McCreary et al. [1993]. The upper layer thickness is not allowed to shallow beyond 10 m or deepen beyond 190 m. The no-slip condition is applied at continental boundaries and the gradient boundary condition [Chapman, 1985] is applied at the open southern boundary at 29°S. The open boundary condition and the restrictions on upper layer thickness force changes in the total mass in the basin; to conserve mass, a uniform correction is applied to the upper layer thickness after each time-step. A linear damper (Rayleigh friction) is applied on the zonal velocity field near the southern boundary; it is required to inhibit the development of large-scale instability along the boundary

⁴These equations are derived in Appendix A.

Table 3.1 Model parameters for the $1\frac{1}{2}$ -layer reduced-gravity model.

Parameter (units)	Symbol	Value
Laplacian mixing coefficient for momentum ($\text{cm}^2 \text{s}^{-1}$)	ν	5×10^7
Laplacian mixing coefficient for thickness ($\text{cm}^2 \text{s}^{-1}$)	κ	1×10^7
Thermal expansion coefficient ($^\circ\text{C}^{-1}$)	α_r	-0.00025
Haline contraction coefficient (PSU^{-1})	α_s	0.00125
Reduced-gravity parameter	$\bar{\Gamma}$	0.0035
Initial upper layer thickness (m)	\bar{H}	100
Minimum upper layer thickness (m)	H_{\min}	10
Maximum upper layer thickness (m)	H_{\max}	190
Linear Kelvin wave speed for $\bar{H} = 100$ m (cm s^{-1})	c	185
Rossby wave speed at 10°N (cm s^{-1})	c_R	12.2
Grid size (km)	$\Delta x, \Delta y$	55
Time step (minutes)	Δt	72

caused by the application of the gradient boundary condition on u . The damper is present only near the boundary, with $\chi = 1 \text{ day}^{-1}$ within 150 km of the boundary, and decreasing to zero linearly in the interval from 150 km to 300 km. There is no corresponding damper on v and H , so that fluid can pass freely through the boundary.

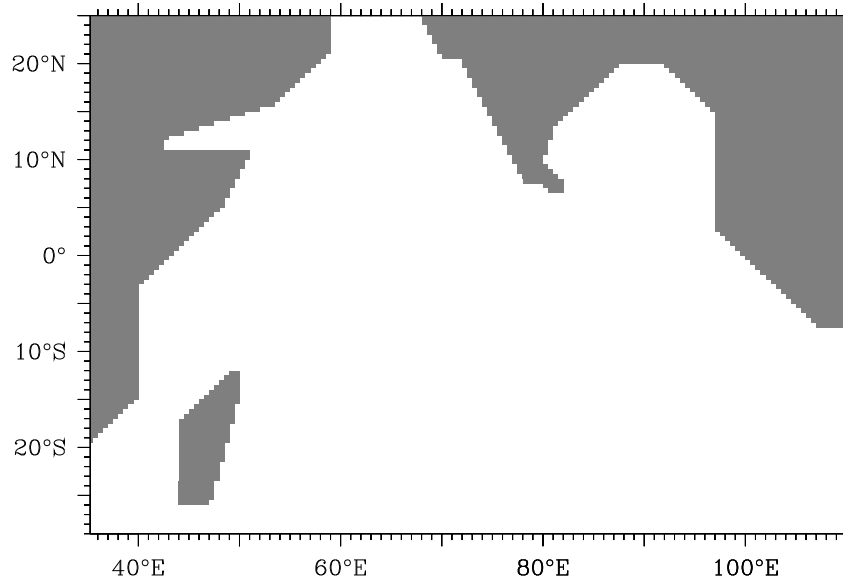
The forcing is derived from the wind-stress climatology of Hellerman and Rosenstein [1983], their wind stress being interpolated linearly to the model grid and then smoothed [McCreary et al., 1993]. Monthly plots of the wind stress in the north Indian Ocean are shown in Figure 3.3. The model is spun up from a state of rest, the winds being ramped up from zero to the appropriate level over five days to damp inertial oscillations. Results discussed below are from the tenth year of the simulation, by when the the model approaches stationarity.

3.3.2 Role of Nonlinearity

Annual sea-level⁵ deviation and velocity over the domain are shown in Figure 3.4 and monthly plots of η and \mathbf{v} are shown in Figure 3.5. The circulation in the eastern Arabian Sea shows a

⁵By annual sea level, we actually mean annual (mean) sea level. It is the mean of monthly sea level over an year. In the model, monthly sea level is computed in two ways. In the figures that show sea-level deviation over the domain, or over the north Indian Ocean, monthly sea level is just the instantaneous sea level in the middle of the model month (day 15). In the figures that show “line-plots” of coastal sea level, it is the mean of daily sea level over a model month (30 days); daily sea level is just the instantaneous sea level at the end of a model day (24 hours). Similarly, by annual velocity, we mean annual mean velocity, the mean of monthly velocity over an year. Monthly velocity is just the instantaneous velocity in the middle of a model month. Note the difference between η_a , which is plotted in the line-plots, and η , which is plotted in the figures that cover the domain or the north Indian Ocean. η_a is the deviation, or anomaly, of the monthly value from the *local* annual mean; η is the deviation from the initial surface. Therefore, the mean of η_a over an year is zero at any location, but that of η is not necessarily so.

Figure 3.2 The domain of the reduced-gravity model for the Indian Ocean. The model domain is identical to that in McCreary et al. [1993]. In some subsequent simulations, the Lakshadweep and Maldive islands are included too; the rest of the domain remains unchanged through all the model results presented in this thesis.



seasonal oscillation in the interface (the model pycnocline), and hence in sea level; a sequence of highs and lows is generated off the west coast of India and the highs and lows propagate westward, as in the altimeter data [Tapley et al., 1994].

In December, the EICC is equatorward; it flows into the westward NMC, which turns around Sri Lanka to join the poleward WICC. In January, a high forms off southwest India. The NMC flows around the high, joining the coastal current, the WICC, at about 12°N . The WICC is poleward north of 12°N and equatorward to the south; the equatorward coastal flow implies coastal downwelling. The high then stretches westward, and the NMC and the high extend across the southern Arabian Sea by March.

By May, the WICC is equatorward all along the coast; it flows into the eastward equatorial jet, which bifurcates near the eastern boundary of the basin. A low forms off southwest India by July. The WICC is equatorward only north of 12°N , where it moves offshore to flow as the Southwest Monsoon Current (SMC) around the western slope of the low; the SMC continues as an eastward current on the southern flank of the low and flows into the Bay of Bengal. South of 12°N , the WICC is poleward, implying coastal downwelling. The low too stretches westward, extending across the southern Arabian Sea by November.

The solution described above reproduces virtually all the significant observed features of the

Figure 3.3 Seasonal cycle of wind stress (dyne cm^{-2}) in the north Indian Ocean. The wind stress is derived from the climatology of Hellerman and Rosenstein [1983]. January marks the end of the northeast monsoon in the Bay of Bengal, where the winds are weak during February–April, these months marking the transition between the northeast and southwest monsoons. The winds weaken over the eastern Arabian Sea too, but they continue to blow from the northeast in the west.

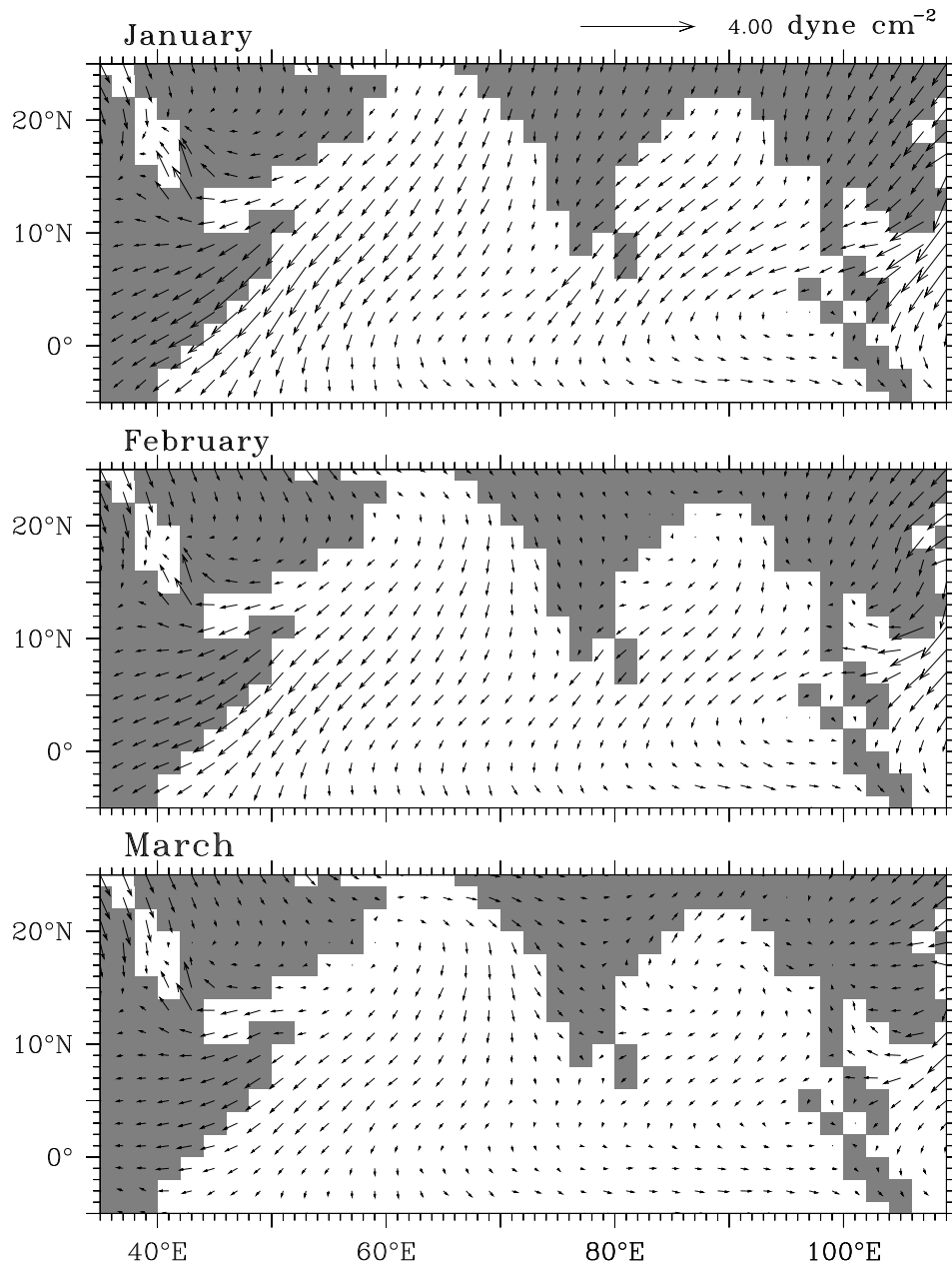


Figure 3.3 (continued) Seasonal cycle of wind stress (dyne cm^{-2}) in the north Indian Ocean. The wind stress is derived from the climatology of Hellerman and Rosenstein [1983]. In April, the winds are at their weakest over the north Indian Ocean. They strengthen in May, blowing from the southwest over the basin, except along the Indian west coast, where they blow from the northwest. The winds are strongest along the east coast of Africa and the central Arabian Sea, where the Findlater jet forms.

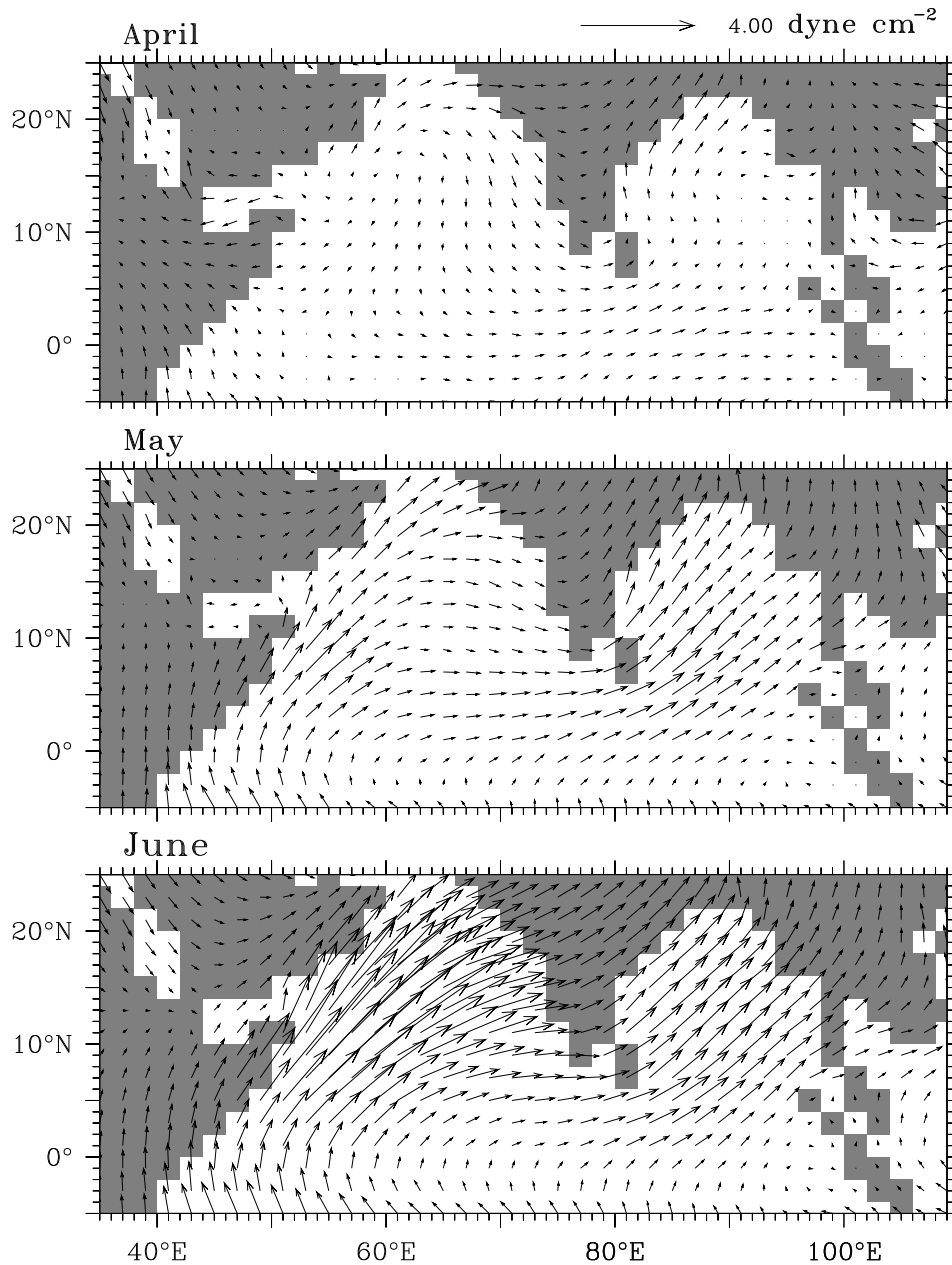


Figure 3.3 (continued) Seasonal cycle of wind stress (dyne cm^{-2}) in the north Indian Ocean. The wind stress is derived from the climatology of Hellerman and Rosenstein [1983]. The southwest monsoon is at its peak in July, with strong winds blowing all over the north Indian Ocean. The winds blow from the southwest over the western Arabian Sea and over the bay, and from the west or northwest over the eastern Arabian Sea. They weaken after July, and October is again a month of transition, with weak winds all over the basin.

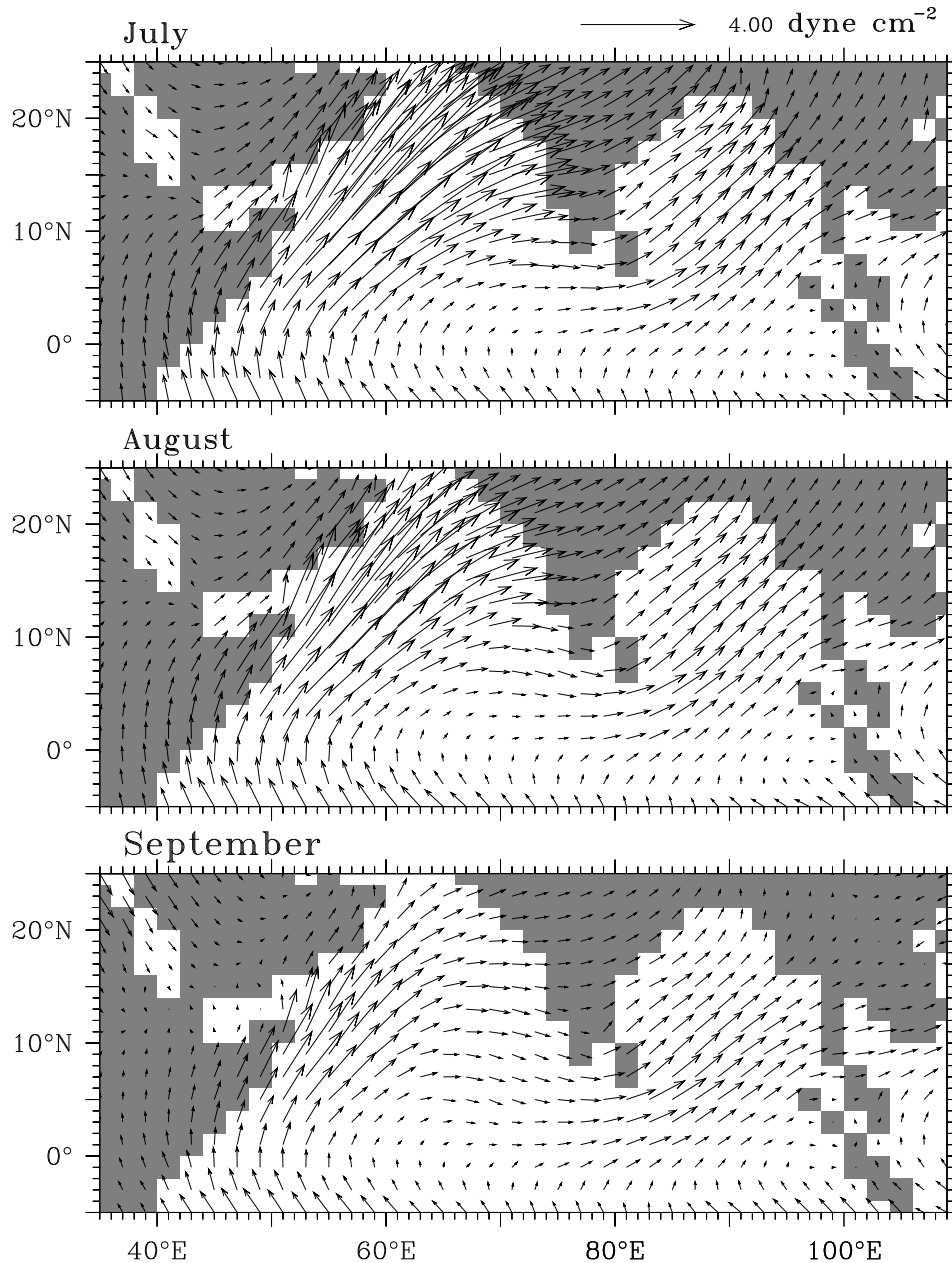


Figure 3.3 (continued) Seasonal cycle of wind stress (dyne cm^{-2}) in the north Indian Ocean. The wind stress is derived from the climatology of Hellerman and Rosenstein [1983]. October is a month of transition between the southwest and northeast monsoons. The winds reverse to blow from the northeast in November, peaking a month later. The northeast monsoon is much weaker than the southwest, resulting in a strong mean wind field over the north Indian Ocean.

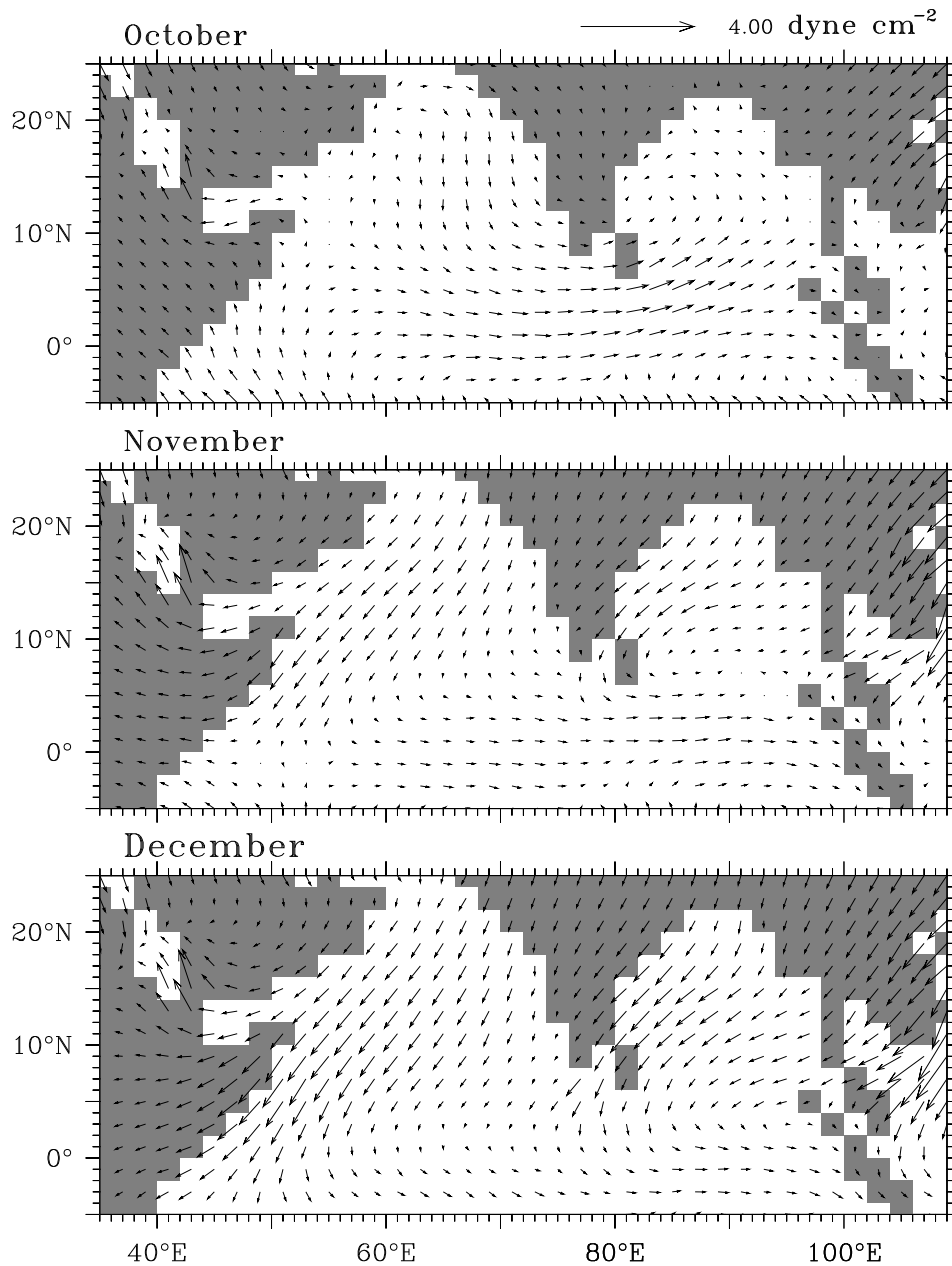


Figure 3.4 Annual sea-level deviation η (cm) and velocity \mathbf{v} (cm s^{-1}) over the model domain. The level of the undisturbed sea surface is removed to obtain the sea-level deviation. This η is different from the η_a that is plotted in the line-plots in Chapters 2 and 4. η_a is the deviation, or anomaly, of the monthly value from the local annual mean. Therefore, the mean of η_a over an year is zero at any location, but that of η is not necessarily so. The solution shows one of the limitations of this model. In the tropical gyre that forms between 5°S and 15°S , the upper layer thickness is at the minimum value, H_{\min} , over a large area. This distorts the momentum balance in the region because the pressure-gradient force, which requires a gradient in H , vanishes, implying a breakdown in the geostrophic balance that should apply in the region and leading to the currents flowing across the contours of H , as in an Ekman balance. A similar distortion occurs in the anticyclonic gyre in the south Indian Ocean, where the upper layer thickness is at its maximum value, H_{\max} , over a large region. Seasonal distortions of this kind occur in the north Indian Ocean too, especially in the strong upwelling regimes off Somalia and Arabia. These distortions are not crucial because their effects are easily seen, but, along with the absence of the Indonesian Throughflow, they make the simulated flow-field different from that observed over a large part of the south Indian Ocean. Hence, our focus in this thesis is on the north Indian Ocean, where the model, despite its simplicity, performs remarkably well; subsequent figures cover only this part of the basin.

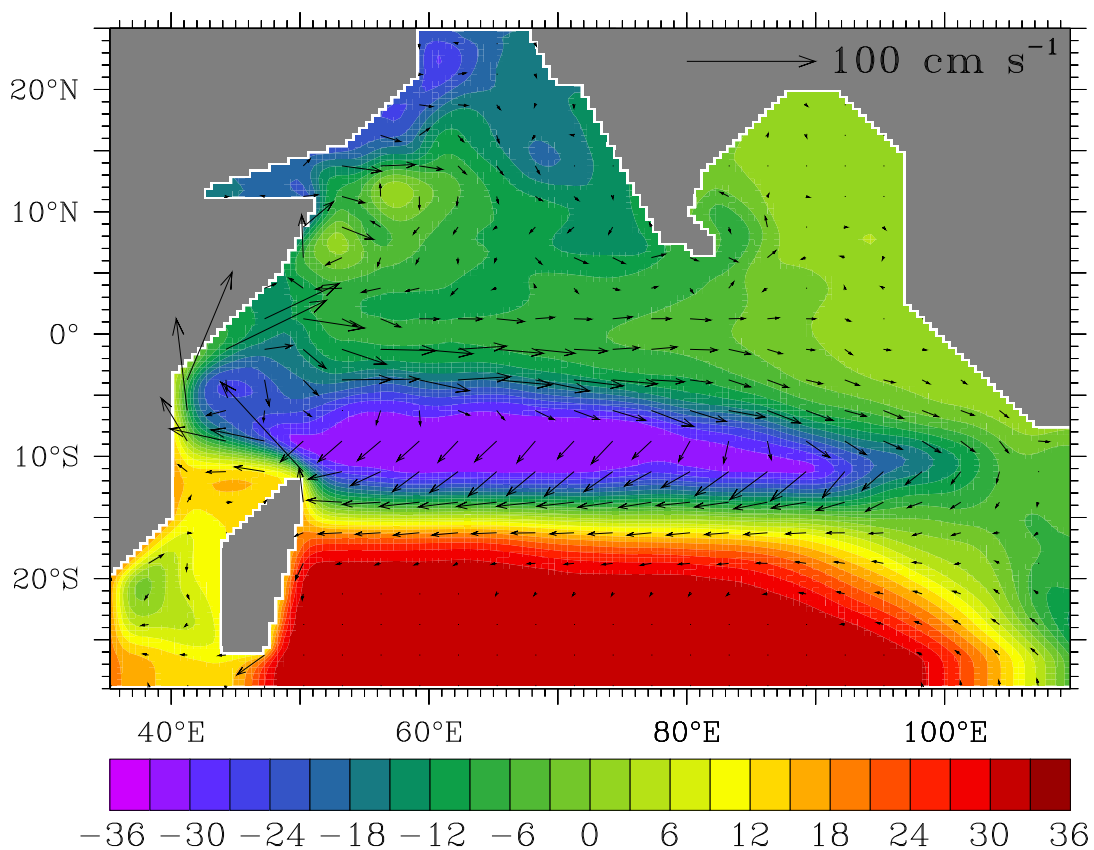


Figure 3.5 Seasonal cycle of surface circulation: nonlinear simulation. Sea-level deviation η (cm) and velocity \mathbf{v} (cm s^{-1}) are shown. In January, the NMC flows around the western flank of the Lakshadweep high off southwest India, joining the poleward WICC at 12°N ; the WICC is equatorward to the south, closing the geostrophic circulation around the high. The high stretches westward, extending across the southern Arabian Sea by April. The EICC flows poleward during February–May, forming the western boundary current of a basin-wide anticyclonic gyre in the Bay of Bengal.

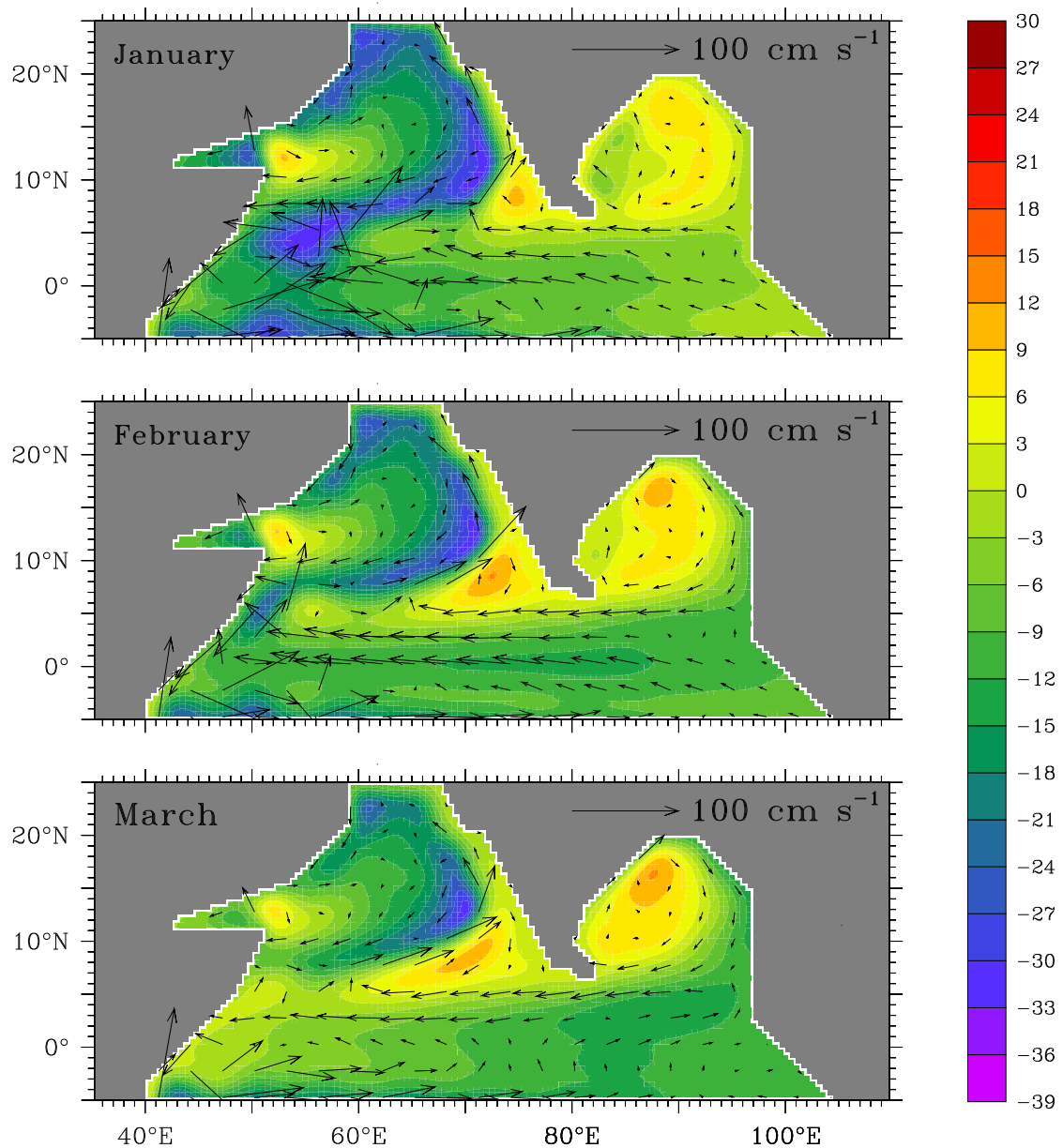


Figure 3.5 (continued) Seasonal cycle of surface circulation: nonlinear simulation. Sea-level deviation η (cm) and velocity \mathbf{v} (cm s^{-1}) are shown. In April, the equatorward WICC off southwest India expands poleward. By June, the WICC is equatorward north of 12°N , where it flows offshore into the SMC, which flows around a low in sea level off southwest India. An eastward jet forms at the equator during April–May. The EICC weakens after April and the anticyclonic gyre vanishes. A weak EICC flows poleward during the southwest monsoon; off Sri Lanka and towards the north of the coast, however, the EICC flows equatorward.

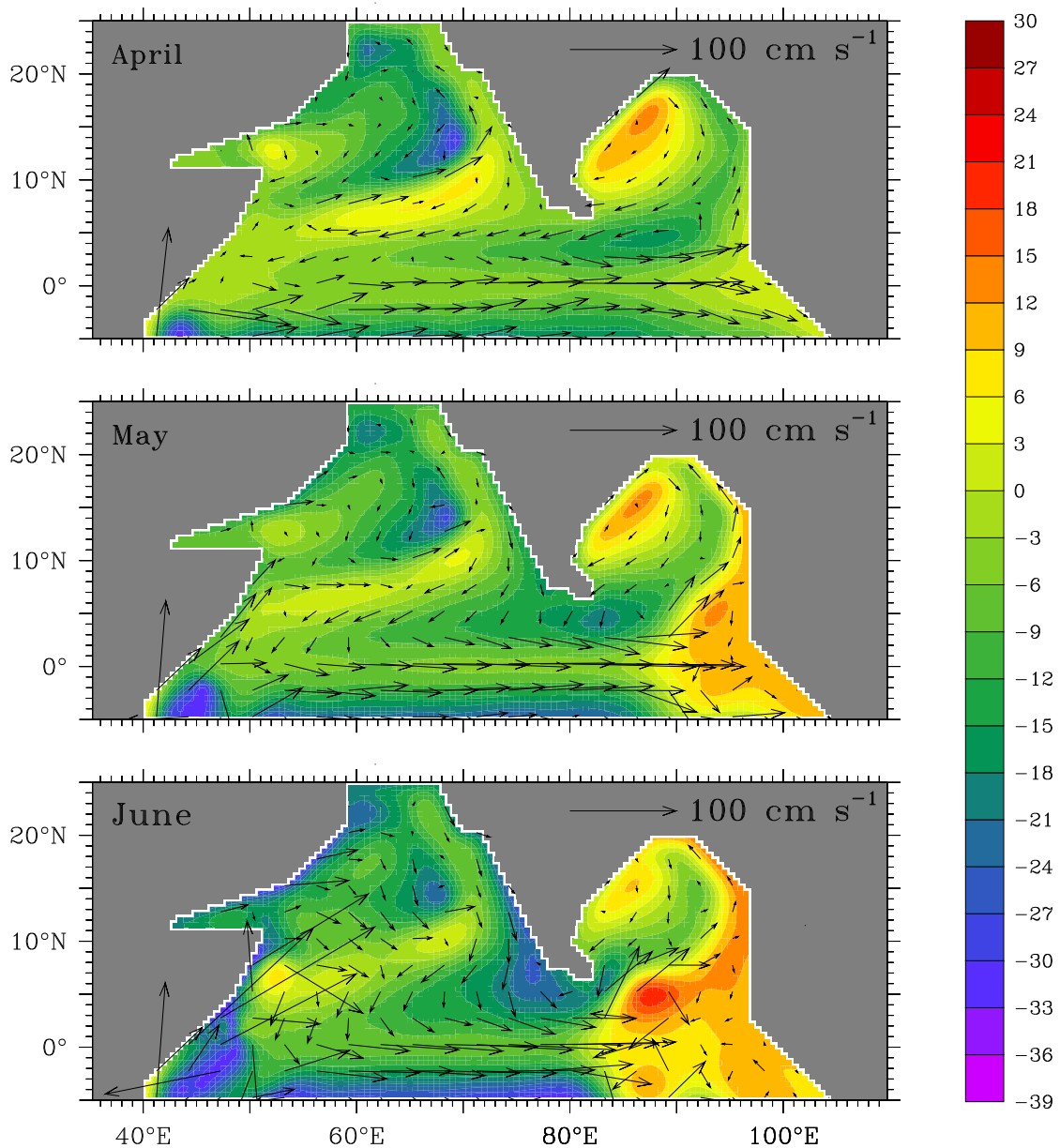


Figure 3.5 (continued) Seasonal cycle of surface circulation: nonlinear simulation. Sea-level deviation η (cm) and velocity \mathbf{v} (cm s^{-1}) are shown. During the southwest monsoon, the Lakshadweep low forms off southwest India and propagates westward. The most vigorous circulation is in the western Arabian Sea, where the Great Whirl forms by July. Another anticyclonic high in sea level, the Socotra high, forms to the north of the Great Whirl. The circulation in the bay lacks organization during the southwest monsoon. The EICC is weak; it is poleward in the south and equatorward in the north and off Sri Lanka.

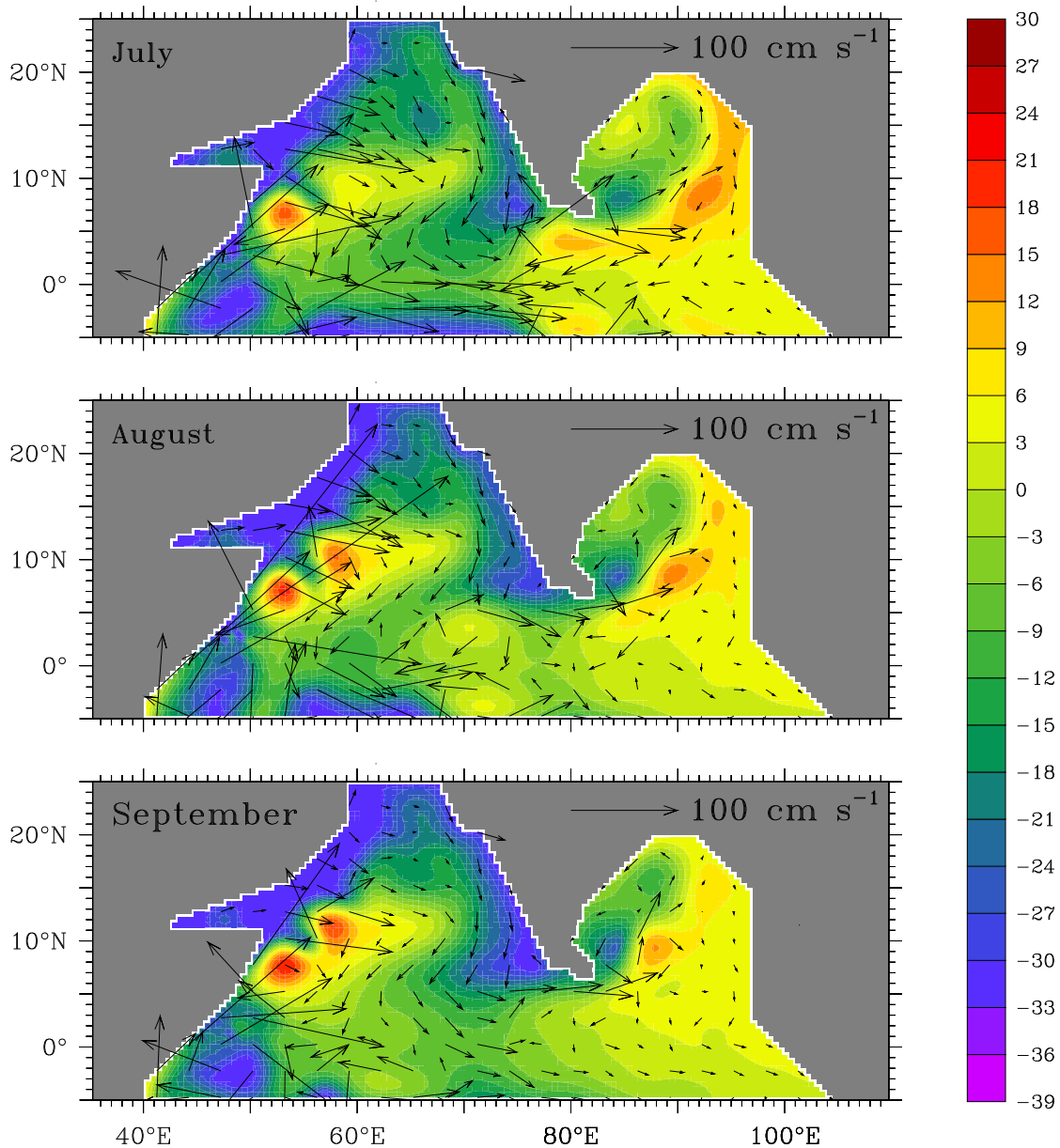


Figure 3.5 (continued) Seasonal cycle of surface circulation: nonlinear simulation. Sea-level deviation η (cm) and velocity \mathbf{v} (cm s^{-1}) are shown. With the collapse of the southwest monsoon in September, the EICC reverses to flow equatorward. It flows into the NMC, which turns around Sri Lanka to join the poleward WICC. In December, the incipient Lakshadweep high is seen off southwest India. Another eastward jet forms at the equator in November, but the model jet does not extend to the eastern boundary.

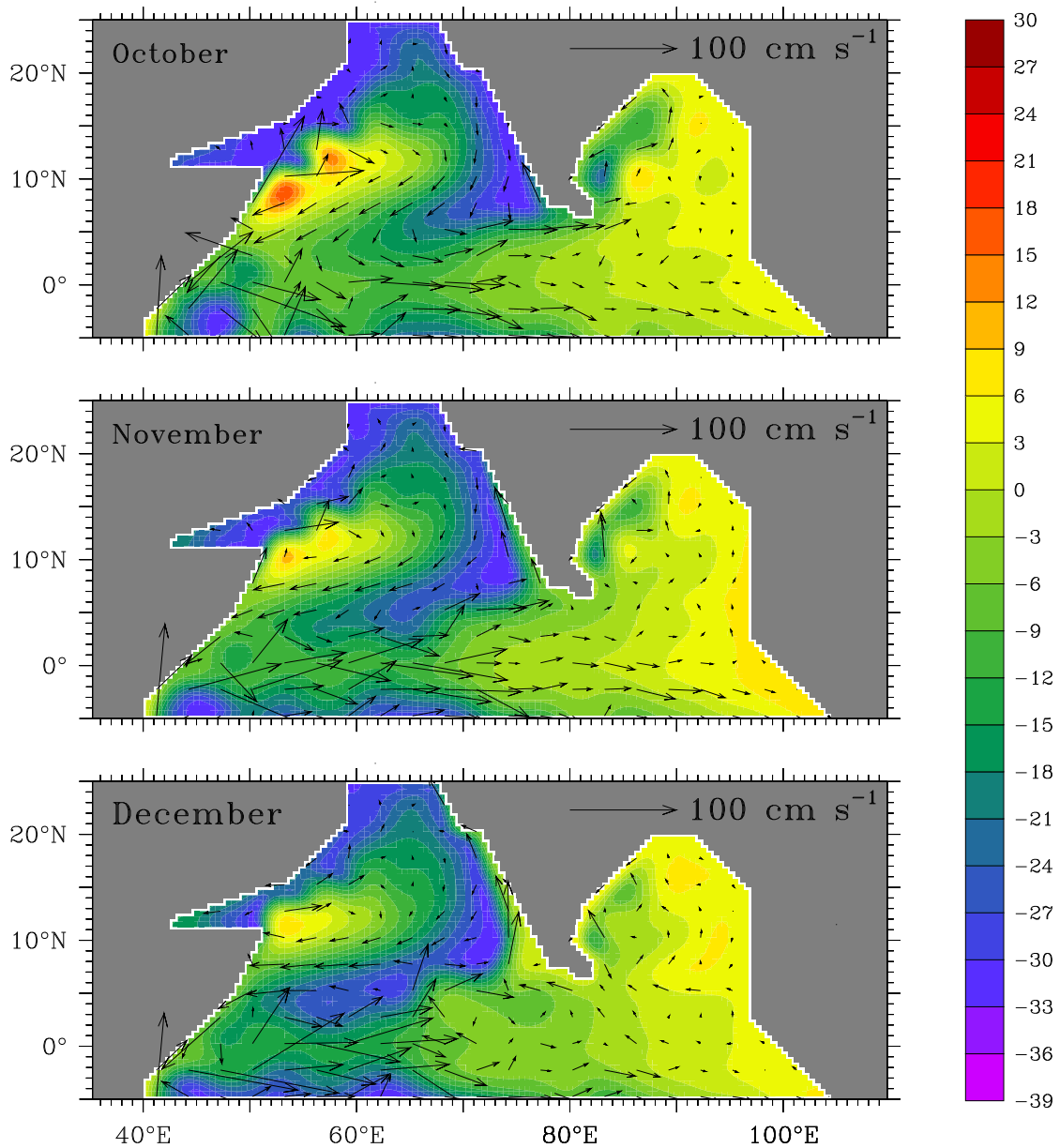


Figure 3.6 Seasonal cycle of surface circulation: linear simulation. Sea-level deviation η (cm) and velocity \mathbf{v} (cm s^{-1}) are shown. The linear solution is virtually identical to the nonlinear solution. Linearization only distorts the highs and lows, stretching them out. The phase speed is constant and the highs and lows propagate at the same speed.

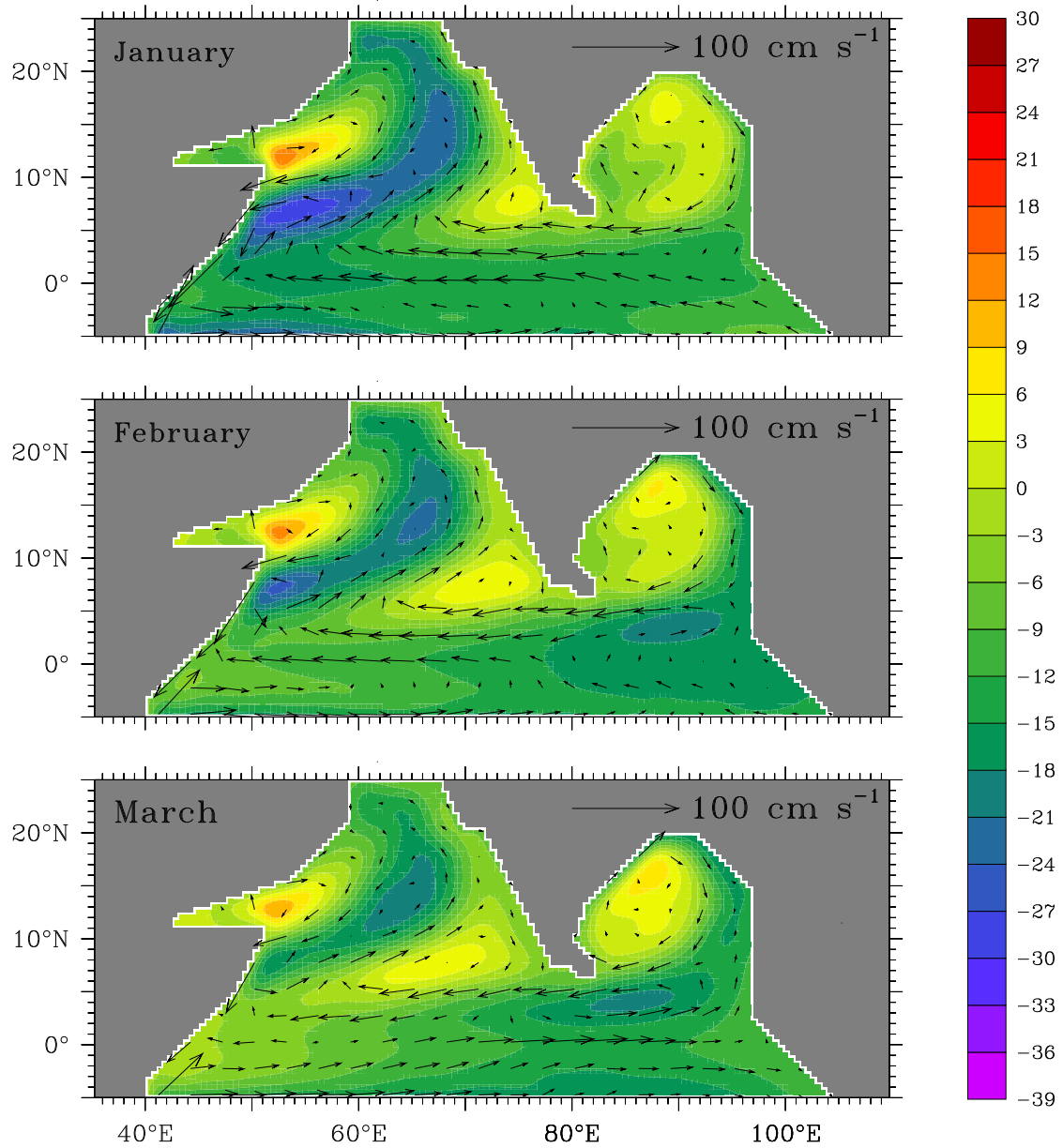


Figure 3.6 (continued) Seasonal cycle of surface circulation: linear simulation. Sea-level deviation η (cm) and velocity \mathbf{v} (cm s^{-1}) are shown. The linear solution is virtually identical to the nonlinear solution. Linearization only distorts the highs and lows, stretching them out. The phase speed is constant and the highs and lows propagate at the same speed.

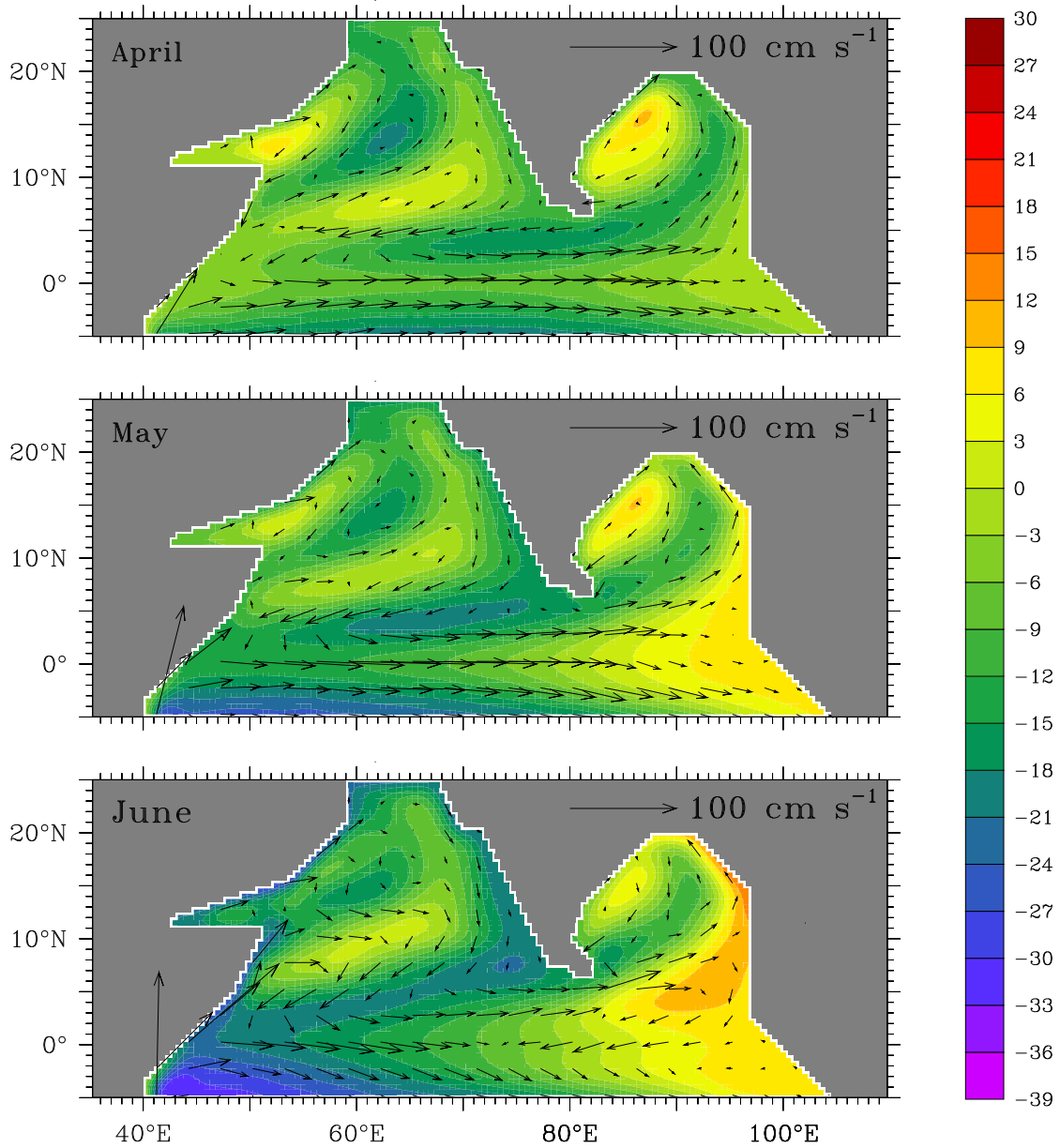


Figure 3.6 (continued) Seasonal cycle of surface circulation: linear simulation. Sea-level deviation η (cm) and velocity \mathbf{v} (cm s^{-1}) are shown. The linear solution is virtually identical to the nonlinear solution, with one major exception. The Great Whirl does not form off Somalia during the southwest monsoon. The two anticyclonic circulations in the region, the Great Whirl and the Socotra high, merge to form a single high in sea level. The Somali Current is also “smoother” in the absence of nonlinearity.

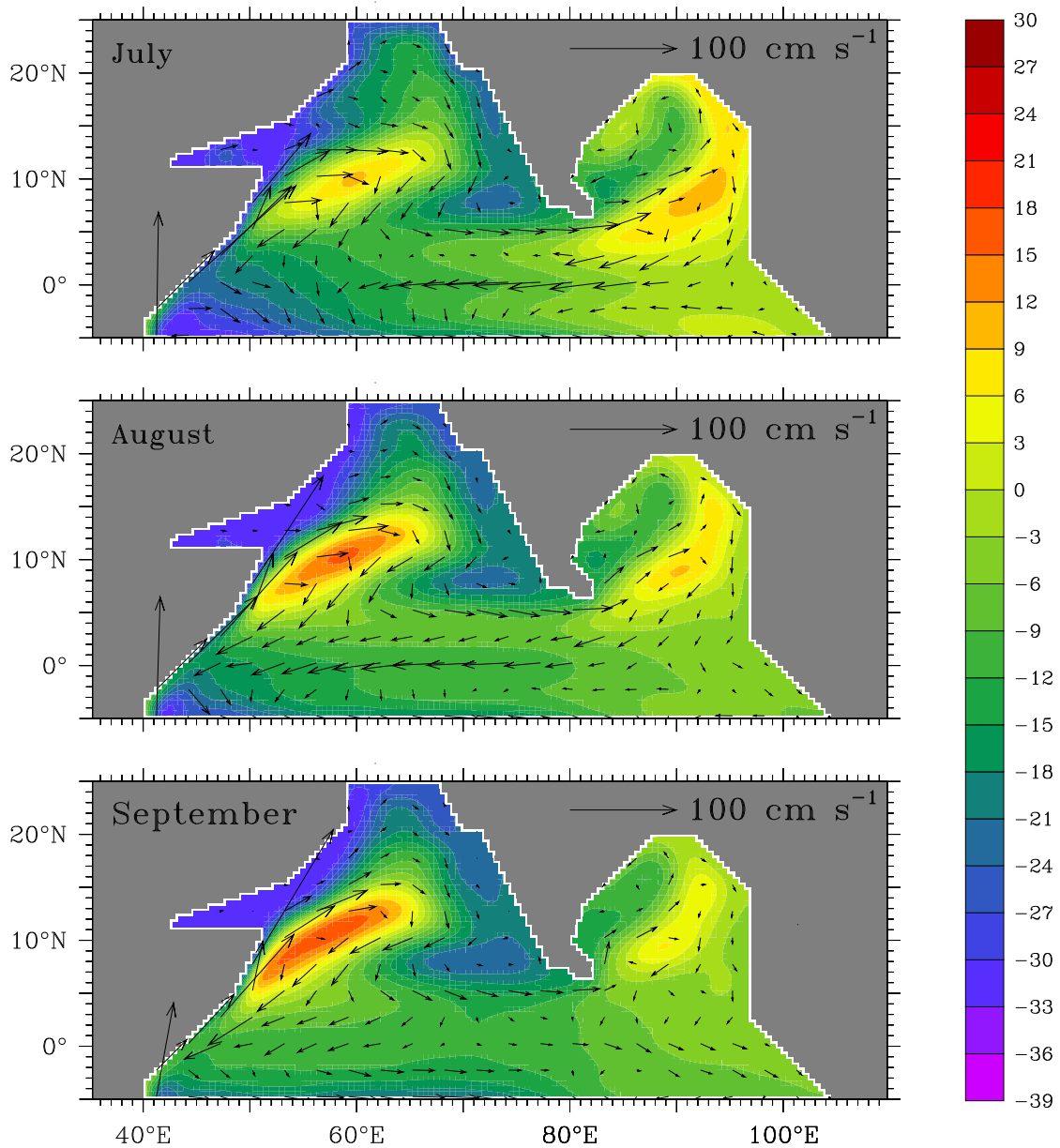
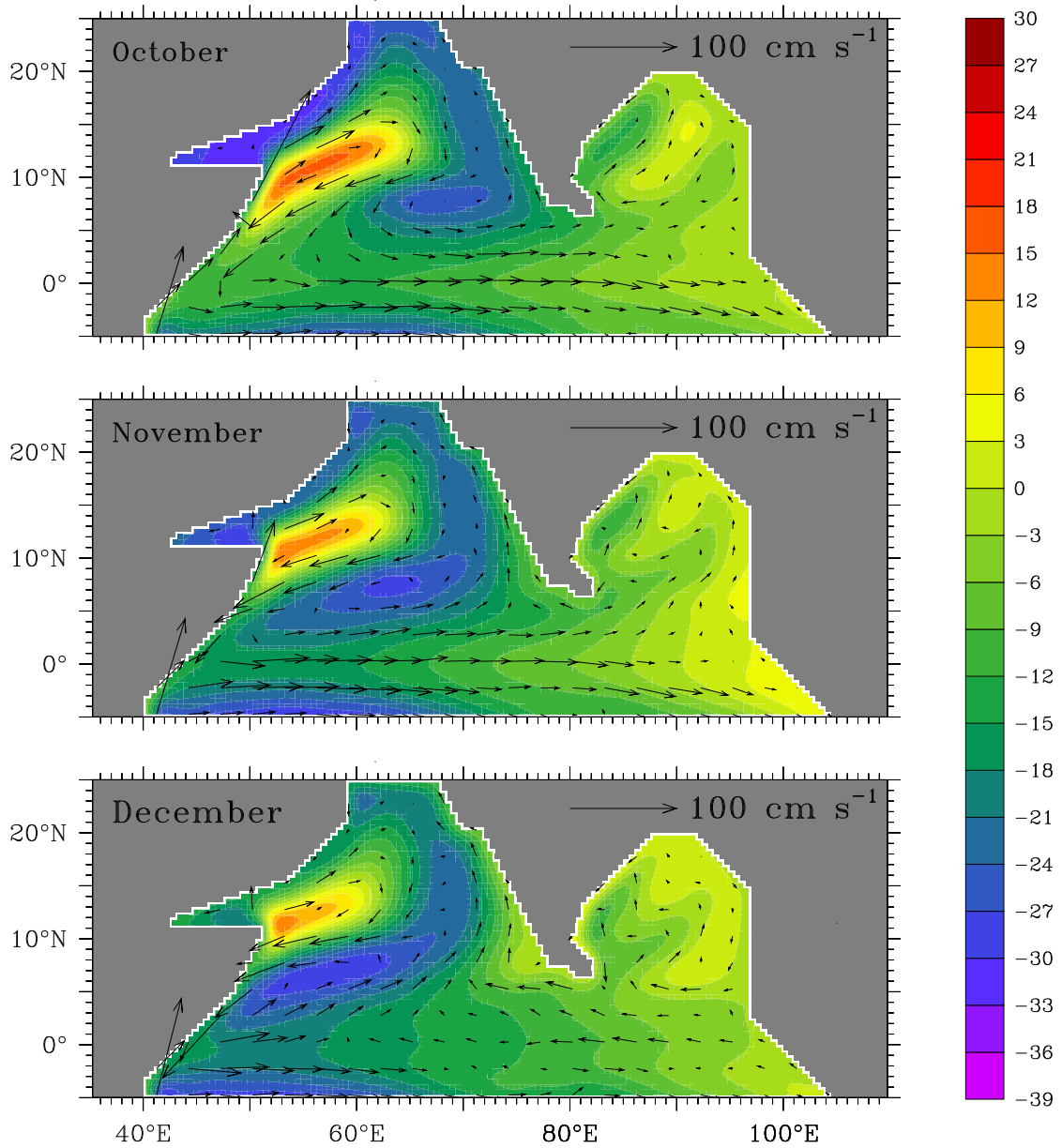


Figure 3.6 (continued) Seasonal cycle of surface circulation: linear simulation. Sea-level deviation η (cm) and velocity \mathbf{v} (cm s^{-1}) are shown. The linear solution is virtually identical to the nonlinear solution. Linearization only distorts the highs and lows, stretching them out. The phase speed is constant and the highs and lows propagate at the same speed.



seasonal cycle of the high and low and of the surface circulation in the vicinity of India. To what extent do these features depend on the nonlinearity in the momentum equations? To answer this question, we linearize model equations⁶. The linear simulation reproduces the seasonal cycle of the Lakshadweep high and low and of the circulation in their vicinity (Figure 3.6). In fact, the linear solution is virtually identical to the nonlinear solution, with one notable exception: the Great Whirl does not form⁷.

This implies that nonlinearity is crucial to the dynamics of the Great Whirl, but not to that of the Lakshadweep high and low. In its absence, they could be generated by the following causes, either individually or in conjunction with the others: Ekman pumping off the southern tip of India, locally forced coastal Kelvin waves or Rossby waves, and Kelvin waves that reach the west coast of India after making their way around Sri Lanka. McCreary et al. [1993] showed the last of these to be particularly important to the circulation off the Indian west coast. Hence, in the following section, we shall study the circulation off southwest India in the presence of only these remotely triggered waves. Before doing so, however, we examine the possible effects of the Lakshadweep and Maldives⁸ islands on the high and low.

3.3.3 Role of Island Chains

We repeat the linear simulation of Section 3.3.2, with but one modification: the Lakshadweep and Maldives island chains are represented as rectangular blocks and the no-slip condition is applied at their boundaries, which correspond roughly to an idealization of the 200 m isobath. Monthly plots of η and v are shown in Figure 3.7. The island chains slow down the westward progress of the high and low. There is also some distortion of the flow-field to the east of the Maldives islands, which are sufficiently long to reflect the westward propagating Rossby waves; this forces a western boundary current along the east coast of the Maldives, and the poleward reflected current strengthens the flow around the high. The Lakshadweep islands, however, are smaller than the meridional wavelength of the Rossby waves, which pass round, or “through”, these islands. Other than these, there are no significant differences introduced by the island chains. They do modify the high and low, but are not, by themselves, responsible for their existence.

⁶See Appendix A, equations (A.13).

⁷Linearization, however, does have other subtle effects. For example, it increases the length scales of highs and lows, stretching them out. It also distorts the phase speeds of the Kelvin and Rossby waves; the highs propagate slower than they do in a nonlinear simulation, and the lows propagate faster.

⁸Like Laccadive, “Maldives” is a distortion of “Maladweep”, literally a “garland of islands”. The Maldives government, however, uses the anglicized form — at least in English — and we see no reason to do otherwise.

Figure 3.7 Effect of the Lakshadweep and Maldive islands on the Lakshadweep high and low. The simulation is linear and identical to that in Figure 3.6, but for the inclusion of the island chains in the Arabian Sea. Plots of sea-level deviation η (cm) and velocity \mathbf{v} (cm s^{-1}) are shown. The presence of the island chains slows down the westward propagation of the Lakshadweep high. The NMC reflects off the Maldives and the current bifurcates, the northern branch flowing poleward, strengthening the flow around the high. The southern branch bends around the Maldives and flows westward along the equator; the axis of the NMC is displaced southward.

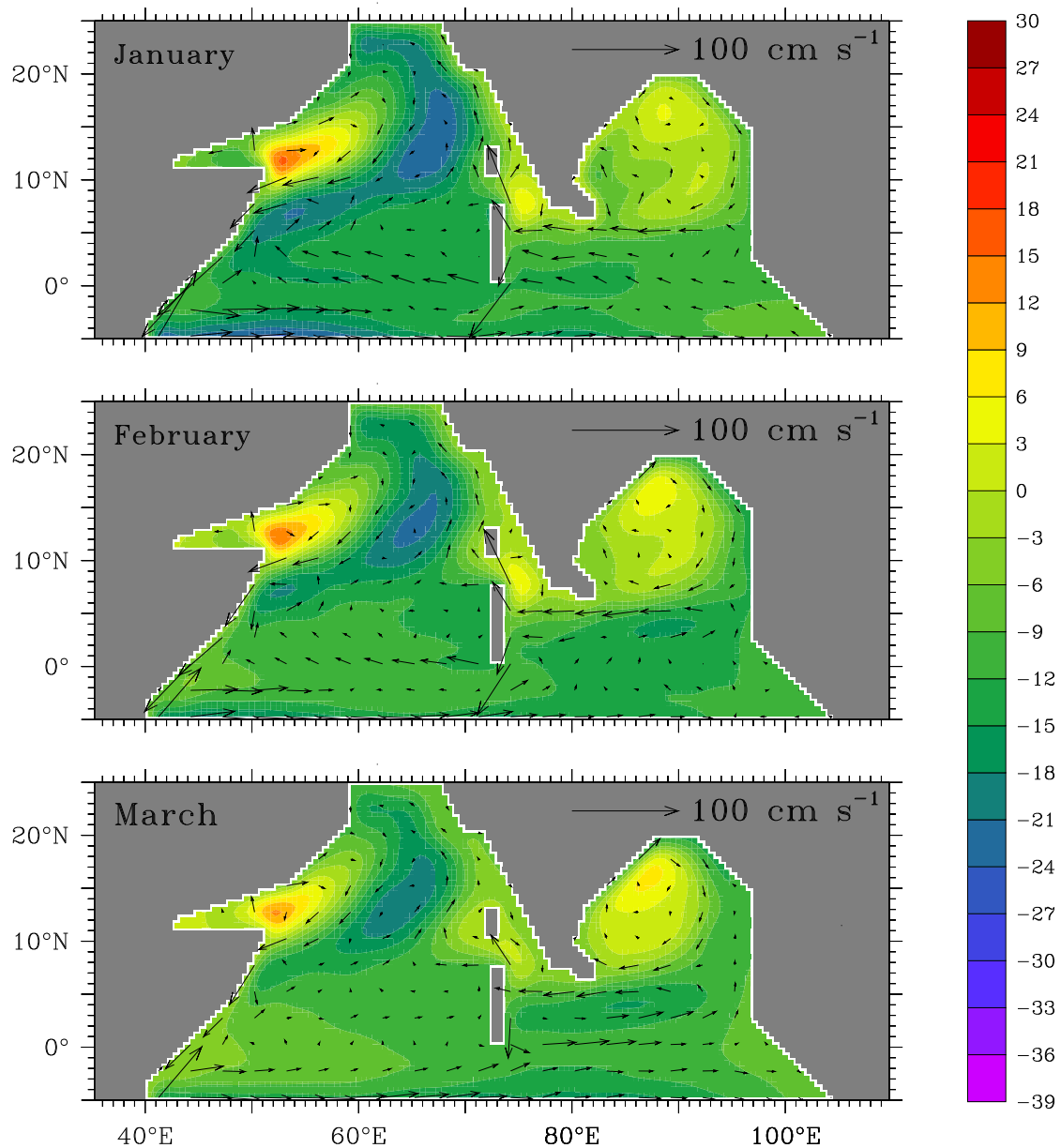


Figure 3.7 (continued) Effect of the Lakshadweep and Maldive islands on the Lakshadweep high and low. The simulation is linear and identical to that in Figure 3.6, but for the inclusion of the island chains in the Arabian Sea. Plots of sea-level deviation η (cm) and velocity \mathbf{v} (cm s^{-1}) are shown. The Lakshadweep islands are smaller than the meridional wavelength of the Rossby waves, which pass round, or “through”, these islands. The islands merely displace the high northward. The Rossby waves in the eastern equatorial Indian Ocean force the SMC in the Bay of Bengal [Vinayachandran and Yamagata, 1998]. These waves also reflect at the east coast of the Maldives, forcing a western boundary current that is a continuation of the equatorward WICC.

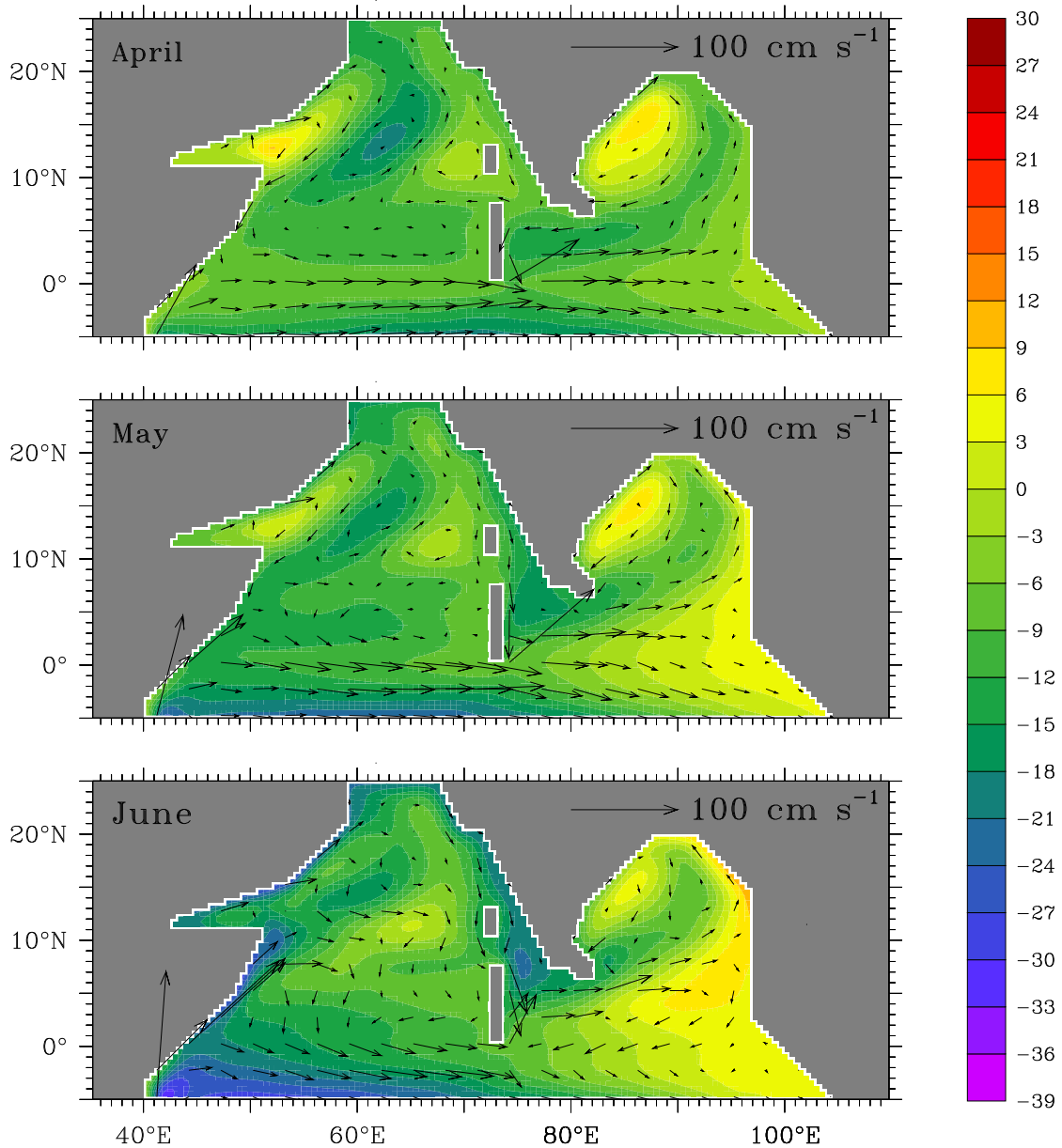


Figure 3.7 (continued) Effect of the Lakshadweep and Maldive islands on the Lakshadweep high and low. The simulation is linear and identical to that in Figure 3.6, but for the inclusion of the island chains in the Arabian Sea. Plots of sea-level deviation η (cm) and velocity \mathbf{v} (cm s^{-1}) are shown. The presence of the islands distorts the SMC; it flows around the Lakshadweep low and turns eastward in the channel between the two island chains. The low propagates faster than in the nonlinear simulation, but is slowed down by the Lakshadweep islands.

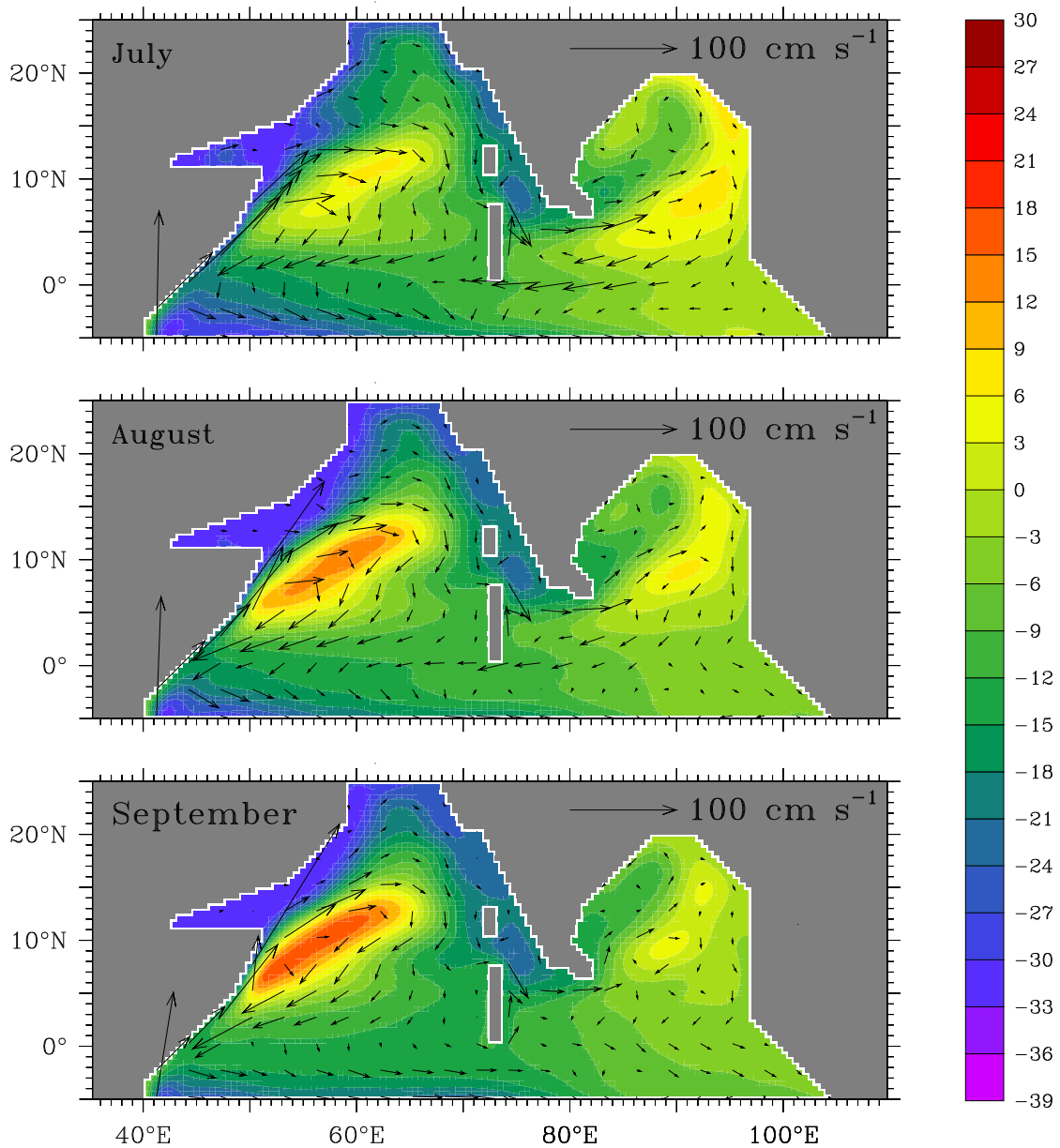
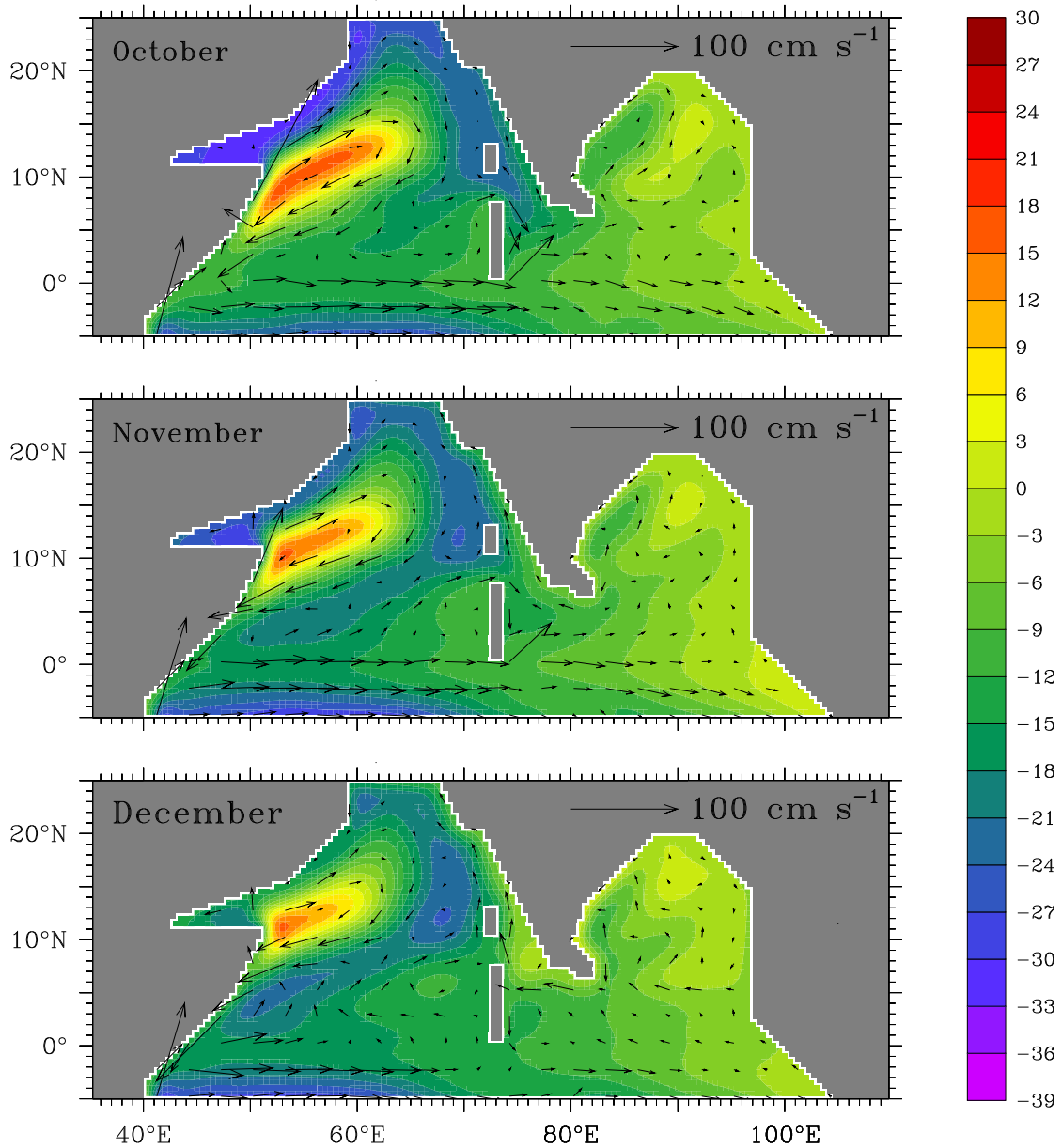


Figure 3.7 (continued) Effect of the Lakshadweep and Maldive islands on the Lakshadweep high and low. The simulation is linear and identical to that in Figure 3.6, but for the inclusion of the island chains in the Arabian Sea. Plots of sea-level deviation η (cm) and velocity \mathbf{v} (cm s^{-1}) are shown. Only a vestige of the SMC remains in October. The NMC begins forming in December and is deflected by the Maldives; the poleward flow strengthens the Lakshadweep high in January.



3.4 Role of Remotely Forced Kelvin Waves

Coastal Kelvin waves in the Bay of Bengal are forced primarily by alongshore winds in the bay or by winds in the equatorial waveguide [McCreary et al., 1993, 1996; Shankar et al., 1996; Yu et al., 1991]. These winds also generate Rossby waves. Our objective in this section is to examine the consequence of a coastal Kelvin wave that reaches the southern tip of India after making its way around Sri Lanka; hence, we use the linearized reduced-gravity model and eliminate all other forcing mechanisms by prescribing an oscillatory boundary forcing. First, we obtain numerical solutions for a realistic basin geometry, but now without any forcing by winds; instead, we generate a coastal Kelvin wave along the east coast of India by prescribing a velocity at the northern boundary of the bay. Second, we obtain an analytic solution for a rectangular basin, in which the arrival of a Kelvin wave at the southern tip of India is mimicked by an oscillating zonal current.

3.4.1 Numerical Experiments

We generate a Kelvin wave along the east coast of India by prescribing a periodic current normal to the northern boundary of the Bay of Bengal in the linearized version of the model. At 20°N , the northern boundary of the bay, the slip-flow condition is used for the zonal velocity, and a periodic meridional (normal) velocity is prescribed as follows:

$$v(x, 20^\circ, t) = -0.4v_0 \cos(\sigma t) |x - 90^\circ|, \quad 87.5^\circ \leq x \leq 90^\circ, \quad (3.2)$$

where x is in degrees longitude, $\sigma = 2\pi \text{ year}^{-1}$, and $v_0 = 40 \text{ cm s}^{-1}$. There is flow into (out of) the bay during October–March (April–September), generating a coastal Kelvin wave of period $T = 2\pi\sigma^{-1}$ along the east coast of India; this wave bends around Sri Lanka and propagates poleward along the west coast, radiating a Rossby wave in the process. The pattern seen off the west coast of India is the result of the coastal Kelvin wave and the Rossby wave. The current associated with the Kelvin wave along the east coast, the model EICC, is connected to the current along the western edge of the Rossby wave.

Monthly plots of η and \mathbf{v} for October–March from the fifth year of the simulation are shown in Figure 3.8, which depicts one half of an annual cycle of events that results in the formation of a high off southwest India. Inflow into the northern bay starts on 1 October, beginning the downwelling phase of the Kelvin wave at the east coast. By mid-October, there is equatorward flow in the northern half of the east coast, but the current is still poleward in the south. This is the continuation of a current along the western edge of a low in the Arabian Sea, which formed off southwest India in July and moved offshore. This current bifurcates at the southern tip of Sri Lanka, part of the flow being deflected poleward along the west coast and the rest bending around Sri Lanka to flow poleward along the east coast. By mid-November, the downwelling phase of the

Figure 3.8 The role of remotely forced Kelvin waves. Sea-level deviation η (cm) and velocity \mathbf{v} (cm s^{-1}) are shown for the linear simulation forced by an oscillatory current at the northern boundary of the Bay of Bengal. The boundary forcing sets up a Kelvin wave along the east coast of India. The downwelling phase begins on 1 October, forcing an equatorward EICC. Off Sri Lanka, the EICC is poleward; it is the continuation of a current that flows along the western edge of a low off southwest India. The low propagates westward and the poleward WICC along its eastern flank extends all along the coast by December.

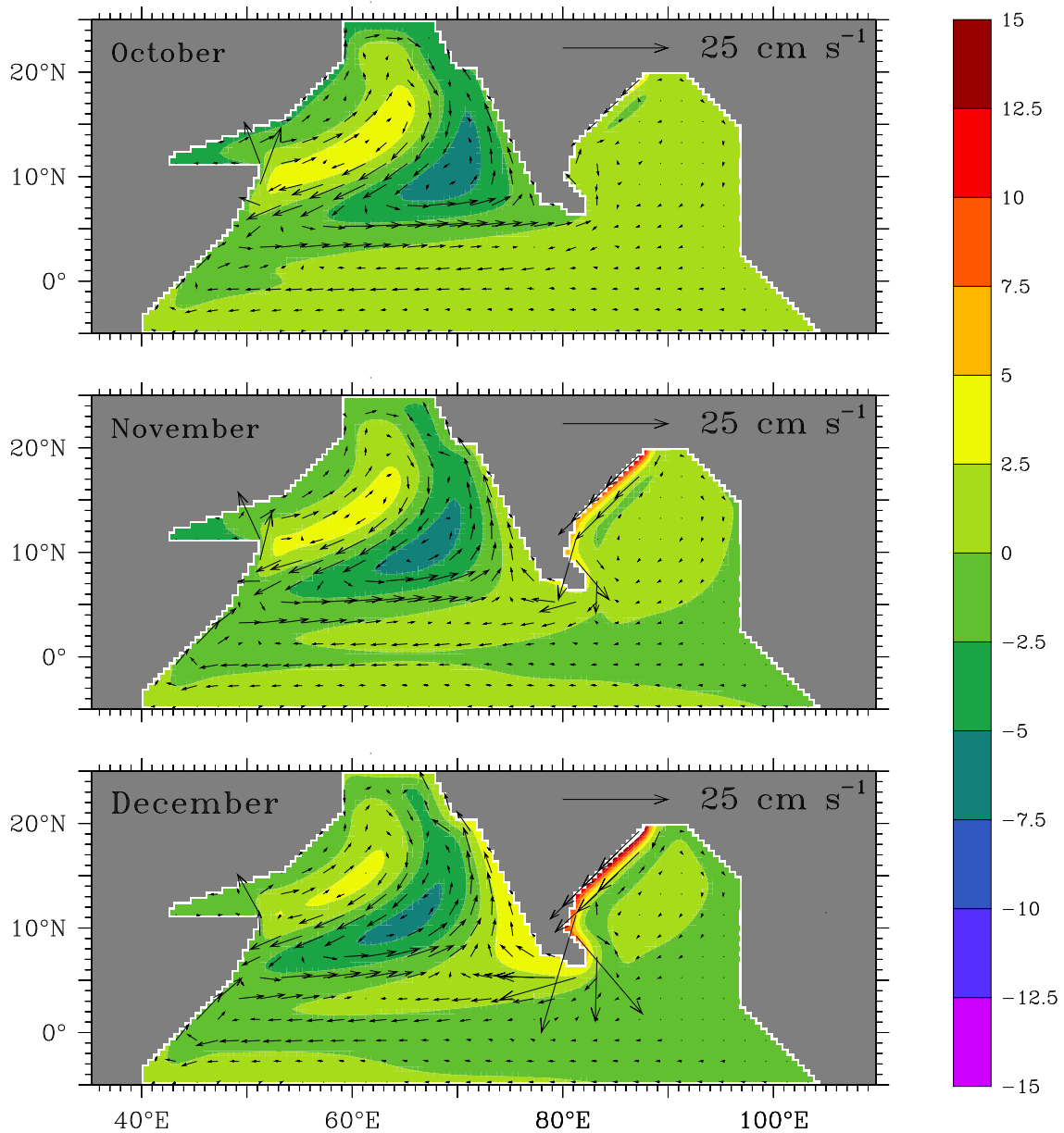
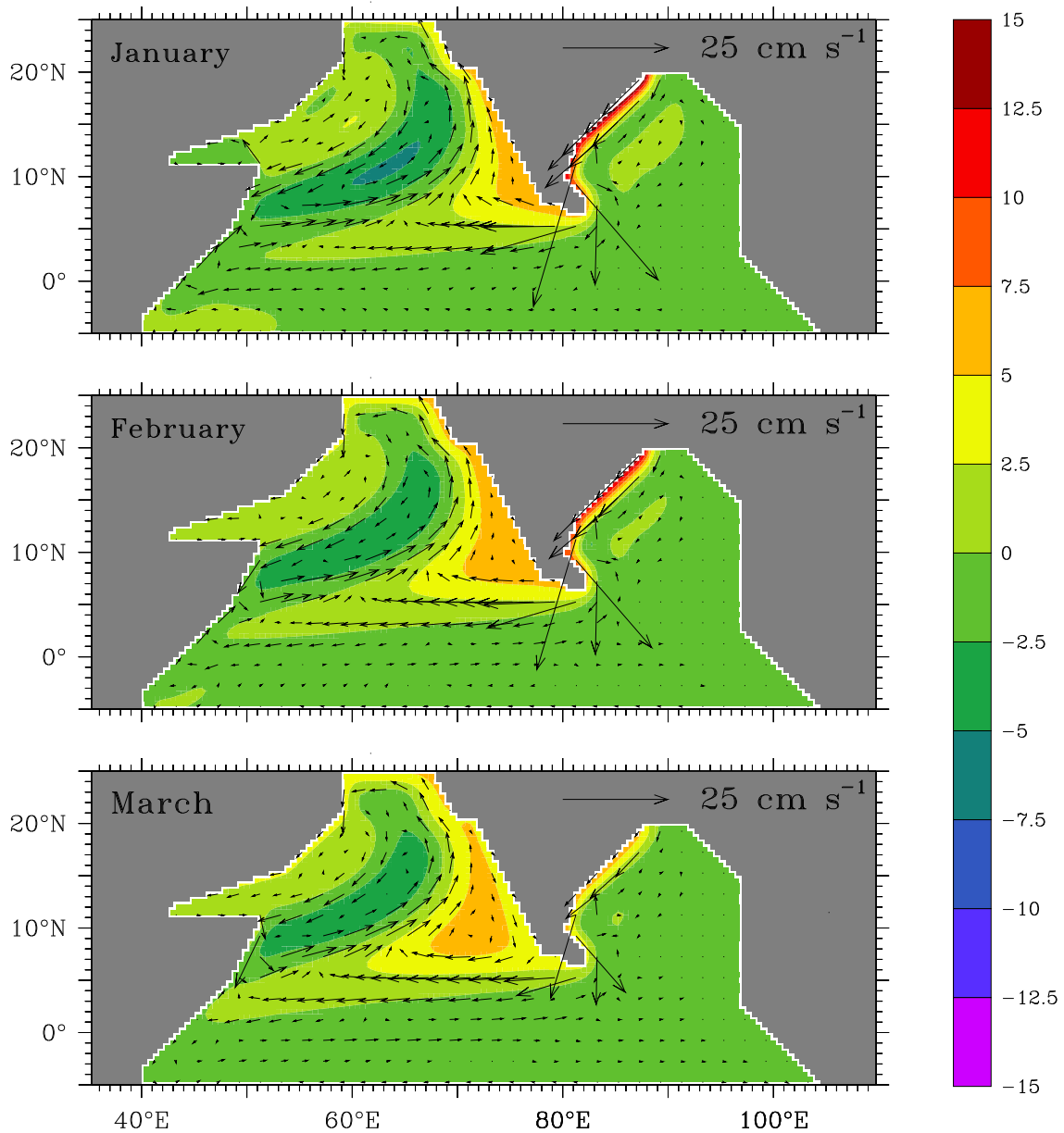


Figure 3.8 (continued) The role of remotely forced Kelvin waves. Sea-level deviation η (cm) and velocity v (cm s^{-1}) are shown for the linear simulation forced by an oscillatory current at the northern boundary of the Bay of Bengal. The Kelvin wave along the east coast bends around Sri Lanka to propagate poleward along the west coast, radiating westward propagating Rossby waves in the process. The high off southwest India is the result of the coastal Kelvin wave and the Rossby waves. It drifts westward together with the Rossby waves that constitute it, spreading across the southern Arabian Sea by March.



Kelvin wave manifests all along the coastline and the equatorward EICC bends around Sri Lanka to flow on as a poleward WICC. Radiation of Rossby waves weakens the WICC off southwest India even as the equatorward EICC peaks (1 January). By February, there is a weak equatorward, upwelling-favourable current off southwest India, closing the circulation around a high. This cycle of events comes to a close by March, when the high drifts westward together with the Rossby waves that constitute it, spreading across the southern Arabian Sea; the Rossby wave signature now appears in the form of a westward current in the vicinity of 5°N and northeastward velocities to the north of this latitude. By the end of March, the inflow in the northern bay vanishes; outflow starts on 1 April, beginning the second half of the annual cycle. This leads to a low off southwest India in August.

Thus, in these experiments, a Kelvin wave along the east coast of India, the model EICC, leads to a symphony of highs and lows off southwest India, these patterns then propagating offshore as Rossby waves.

3.4.2 Analytic Solution

We now obtain a simple analytic solution to show that all the crucial elements of the observed high and low and the associated currents along the west coast of India are contained in coastal Kelvin and equatorial Rossby waves, both of which arise from linear dynamics on an equatorial β -plane. We use the linearized reduced-gravity model without wind stress forcing and replace Laplacian friction by Rayleigh friction. The equations, derived in Appendix A, are

$$i\omega u - fv + g\bar{\Gamma}h_x = 0, \quad (3.3a)$$

$$i\omega v + fu + g\bar{\Gamma}h_y = 0, \quad (3.3b)$$

$$i\omega h + \bar{H}(u_x + v_y) = 0, \quad (3.3c)$$

$$\eta = \bar{\Gamma}h, \quad (3.3d)$$

where $H = \bar{H} + h$, $c = (g\bar{\Gamma}\bar{H})^{\frac{1}{2}}$ is the speed of the Kelvin wave, and

$$i\omega = \frac{\partial}{\partial t} + r = i\sigma + r. \quad (3.4)$$

r is the Rayleigh friction coefficient and has units of s^{-1} ; it is equivalent to Ac_n^{-2} in McCreary [1981] and Shankar and Shetye [1997].

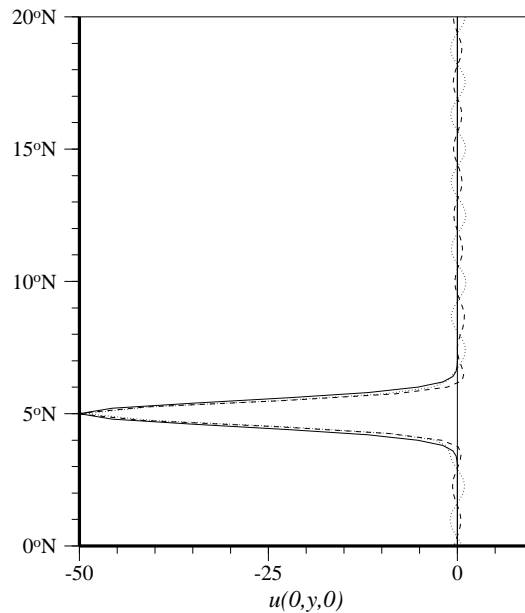
The boundary condition in the meridional direction is that there are no sources of energy at high latitudes: no energy is brought into the ocean by a high-latitude source of Kelvin waves. At the eastern boundary, we impose the condition

$$u(0, y, t) = \Re \left[u_0 e^{-\delta_1 (\zeta - \zeta_0)^2 + i\omega t} \right], \quad (3.5)$$

where $\zeta = \alpha_0 y$, $\alpha_0^2 = \beta/c$, and $\delta_1 > 0$.

For sufficiently large δ_1 , (3.5) represents a narrow zonal flow into or out of the domain, the zonal velocity being nearly zero a short distance north or south of the axis of symmetry y_0 . The $u \approx 0$ condition to the north of the flow mimics a closed eastern boundary and represents the Indian west coast; the $u \approx 0$ condition to the south of the flow mimics an open boundary with negligible flow and represents the open ocean to the south of Sri Lanka (see Figure 3.9).

Figure 3.9 The eastern boundary condition for the analytic solution, showing $u(0, y, 0)$ (cm s^{-1}) for the Gaussian profile in (3.5) (solid curve) and for periods $T = 360$ days (dashed curve) and $T = 30$ days (dotted curve). 7500 meridional modes were summed over to obtain the dashed and dotted curves, which merge in the region where velocity is not negligible, indicating the degree of accuracy achieved in satisfying the eastern boundary condition. At the eastern boundary, the dashed portion is open and the rest is closed.



The homogeneous solution to (3.3), subject to the condition (3.5), is given by [McCreary, 1980, 1981]

$$u_m = B_m [K_m \phi_{m+1} - \phi_{m-1}] e^{ik_m(x-x_e)}, \quad (3.6a)$$

$$v_m = B_m \left[\left(\frac{t}{c\alpha_0} \right) \frac{(ck_m - \omega)}{\frac{1}{(m/2)^2}} \phi_m \right] e^{ik_m(x-x_e)}, \quad (3.6b)$$

$$h_m = B_m \left(\frac{c}{g\Gamma} \right) [K_m \phi_{m+1} + \phi_{m-1}] e^{ik_m(x-x_e)}, \quad (3.6c)$$

where $m = 1, 2, 3, \dots$; x_e represents the eastern boundary,

$$K_m = \left(\frac{ck_m - \omega}{ck_m + \omega} \right) \left(\frac{m+1}{m} \right)^{\frac{1}{2}},$$

$$k_m = \frac{\beta}{2\omega} \left(1 - \left[1 - \frac{4\omega^2}{\beta^2} \left(\alpha_m^2 - \frac{\omega^2}{c^2} \right) \right]^{\frac{1}{2}} \right),$$

and $\alpha_m = \alpha_0(2m+1)$. The ϕ_m are the normalized Hermite functions, given by [McCreary, 1981]

$$\phi_m(\zeta) = \frac{(-1)^m}{(2^m m! \pi^{\frac{1}{2}})^{\frac{1}{2}}} e^{\zeta^2/2} \frac{d^m}{d\zeta^m} e^{-\zeta^2}. \quad (3.7)$$

$m = -1$ and $m = 0$ represent the equatorial Kelvin and Yanai waves in the terminology used by McCreary [1981]; both propagate eastward and hence, $B_{-1} = B_0 = 0$. The coefficients with $m \geq 1$ represent westward propagating Rossby waves with complex wavenumber k_m . Since

$$u(0, y, t) = \Re \left[\sum_{m=1}^M u_m e^{i\omega t} \right], \quad (3.8)$$

and the ϕ_m are orthogonal functions, we multiply both sides of (3.5) and (3.8) by ϕ_m and integrate over $\zeta = (-\infty, \infty)$ to obtain the relation

$$B_m = K_{m-2} B_{m-2} - u_0 (2\pi\delta_2)^{\frac{1}{2}} (1 - 2\delta_2)^{(m-1)/2} e^{(\zeta_{00}^2 - \delta_1 \delta_2 \zeta_0^2)} \phi_{m-1}(\zeta_{00}), \quad (3.9)$$

where

$$\delta_2 = \frac{1}{2(\delta_1 + \frac{1}{2})},$$

$$\zeta_{00} = \frac{2\delta_1 \delta_2 \zeta_0}{(1 - 2\delta_2)^{\frac{1}{2}}},$$

and we have used [Gradshteyn and Ryzhik, 1965, p. 838]

$$\int_{-\infty}^{\infty} e^{-\frac{(\zeta-\zeta_1)^2}{2\delta_2}} H_m(\zeta) d\zeta = (2\pi\delta_2)^{\frac{1}{2}} (1-2\delta_2)^{\frac{m}{2}} H_m \left[\frac{\zeta_1}{(1-2\delta_2)^{\frac{1}{2}}} \right], \quad (3.10a)$$

where $\zeta_1 = 2\delta_1\delta_2\zeta_0$ and

$$H_m(\zeta) = (-1)^m e^{\zeta^2} \frac{d^m}{d\zeta^m} e^{-\zeta^2}. \quad (3.10b)$$

The recursion relation [McCreary, 1981]

$$\zeta\phi_m(\zeta) = \left(\frac{m+1}{2}\right)^{\frac{1}{2}} \phi_{m+1}(\zeta) + \left(\frac{m}{2}\right)^{\frac{1}{2}} \phi_{m-1}(\zeta) \quad (3.10c)$$

and (3.9) are used to estimate the complex coefficients B_m , which when substituted in (3.6) give the required solution.

We compute the solution for the parameters $\bar{H} = 100$ m and $\bar{\Gamma} = 0.0035$, which imply $c = 185$ cm s⁻¹, and $r = 2.1 \times 10^{-9}$ s⁻¹. The solution is not sensitive to the choice of r . To prescribe the eastern boundary condition (3.5), we choose $\delta_1 = 20$, $y_0 = 5^\circ\text{N}$, and $u_0 = -40$ cm s⁻¹. Accurate reproduction of the Gaussian velocity profile requires a large value of M in (3.8); the degree of accuracy achieved in satisfying the boundary condition using $M = 7500$ is shown in Figure 3.9.

The solution for a zonal current oscillating with a period $T = 2\pi\sigma^{-1} = 360$ days is shown in Figure 3.10. In the solution, $t = 0$ corresponds to 1 January, when the flow into the basin, the model EICC⁹, peaks. Figure 3.10 depicts how η and \mathbf{v} evolve during one half of an annual cycle. The close resemblance of the analytic solution to the evolution depicted in Figure 3.8 implies that it captures the essential elements of the dynamics. As in the numerical experiment with a boundary forcing in lieu of wind stress, the current at the coast reverses to flow equatorward and a high forms by 1 January, when the inflow into the basin peaks. The changes in current and sea level propagate into the open sea. A low forms in like fashion during the second half of the cycle.

The solution for a zonal current of period 60 days is shown in Figure 3.11. The pattern of evolution is virtually identical to that for the annual harmonic. Figure 3.11, however, illustrates two aspects of the dynamics not evident in Figure 3.10. First, the time scale associated with the evolution is a sixth that for the annual harmonic; consequently, the zonal length scale (equal to the product of T and the Rossby wave speed) of patterns seen in the solution is much smaller. Therefore, a series of highs and lows are spread zonally, one high and one low forming at the eastern boundary during one cycle of period T and then migrating westward. Second, the Rossby waves are trapped south of a critical latitude

$$y_c = \frac{c}{2\sigma}. \quad (3.11)$$

⁹Strictly, it is the NMC or the SMC that the zonal current represents.

Propagating Rossby waves cannot exist poleward of the critical latitude¹⁰, which is 7° for $T = 60$ days. The critical latitude for $T = 360$ days is 42° , well to the north of the northern boundary of the Arabian Sea; therefore, the waves are not trapped in Figures 3.8 and 3.10.

An extreme case of trapping is shown in Figure 3.12, which depicts the solution for $T = 30$ days. The critical latitude for this period is 3.5° , to the south of the axis of the zonal current at the eastern boundary. Therefore, Rossby wave radiation is impossible, and the high and low do not form; the zonal flow is deflected north and propagates as a coastal Kelvin wave.

Rossby-wave trapping implies that the location of the southern tip of Sri Lanka is crucial in determining the period of oscillations that will migrate westward into the Arabian Sea from the west coast of the India. At the southern tip of Sri Lanka, 6°N , the critical period is 52 days. Only those disturbances from the Bay of Bengal that have a larger period can generate westward propagating Rossby waves and contribute to the high and low; those with smaller periods will remain trapped at the west coast of Sri Lanka and India. This critical period, however, depends on the Kelvin wave speed c , which depends on stratification and, hence, is a function of time and space¹¹. Therefore, the partition between disturbances that are trapped at the coast and those that propagate offshore will not be defined as sharply as in this simple model.

The location of the southern tip of Sri Lanka, at about 6°N , is crucial for another reason too. The internal radius of deformation at this latitude is about 200 km; the radius of deformation at the equator, the e -folding length scale of the equatorial Kelvin wave, is about 300 km. Therefore, the coastal waveguide in which the Kelvin wave propagates is distinct from the equatorial waveguide. This permits the Kelvin waves from the Bay of Bengal to pass unhindered into the Arabian Sea, linking the dynamics of the two basins.

The equatorial waveguide is connected to the bay at its eastern boundary. This link arises as a consequence of the reflection of the equatorial Kelvin wave at the eastern boundary of the basin; the reflected wave is a summation over several meridional modes of the westward propagating Rossby wave, these being required to satisfy the condition of no normal flow at the boundary [Moore, 1968]. The higher meridional modes were shown by Moore to be equivalent to a coastal Kelvin wave, which carries a part of the incident energy poleward along the coast in both hemispheres. This Kelvin wave is trapped at the coast poleward of the critical latitude; equatorward of this latitude, westward radiation of energy is possible, and the coastal Kelvin wave is inseparable from the Rossby wave. The same phenomenon is seen off the Indian west coast. For the seasonal cycle, it is the annual and semiannual harmonics that are most important. The critical latitudes for these periods are 42° and 21° , respectively; the former lies poleward of the northern boundary

¹⁰The critical latitude is actually smaller (farther south) for the Indian west coast because the boundary is not meridional [Clarke and Shi, 1991]. The critical latitude for a non-meridional boundary is $y_c = \frac{c \cos \theta}{2\sigma}$, where θ is the deviation of the coast from the meridian. For the Indian west coast, $\theta \approx 18^\circ$, which gives a factor of 0.95.

¹¹Shankar and Shetye [1997] obtained different values for the critical latitude and period because they used a higher value of c (250 cm s^{-1}).

Figure 3.10 Analytic solution for $T = 360$ days (annual harmonic). Sea-level deviation η (cm) and velocity \mathbf{v} (cm s^{-1}) are plotted for half the annual cycle. As in Figure 3.8, the current at the coast reverses to flow equatorward and a high forms by 1 January, when the inflow into the basin peaks. The changes in current and sea level propagate into the open sea. A low forms in like fashion during the second half of the cycle.

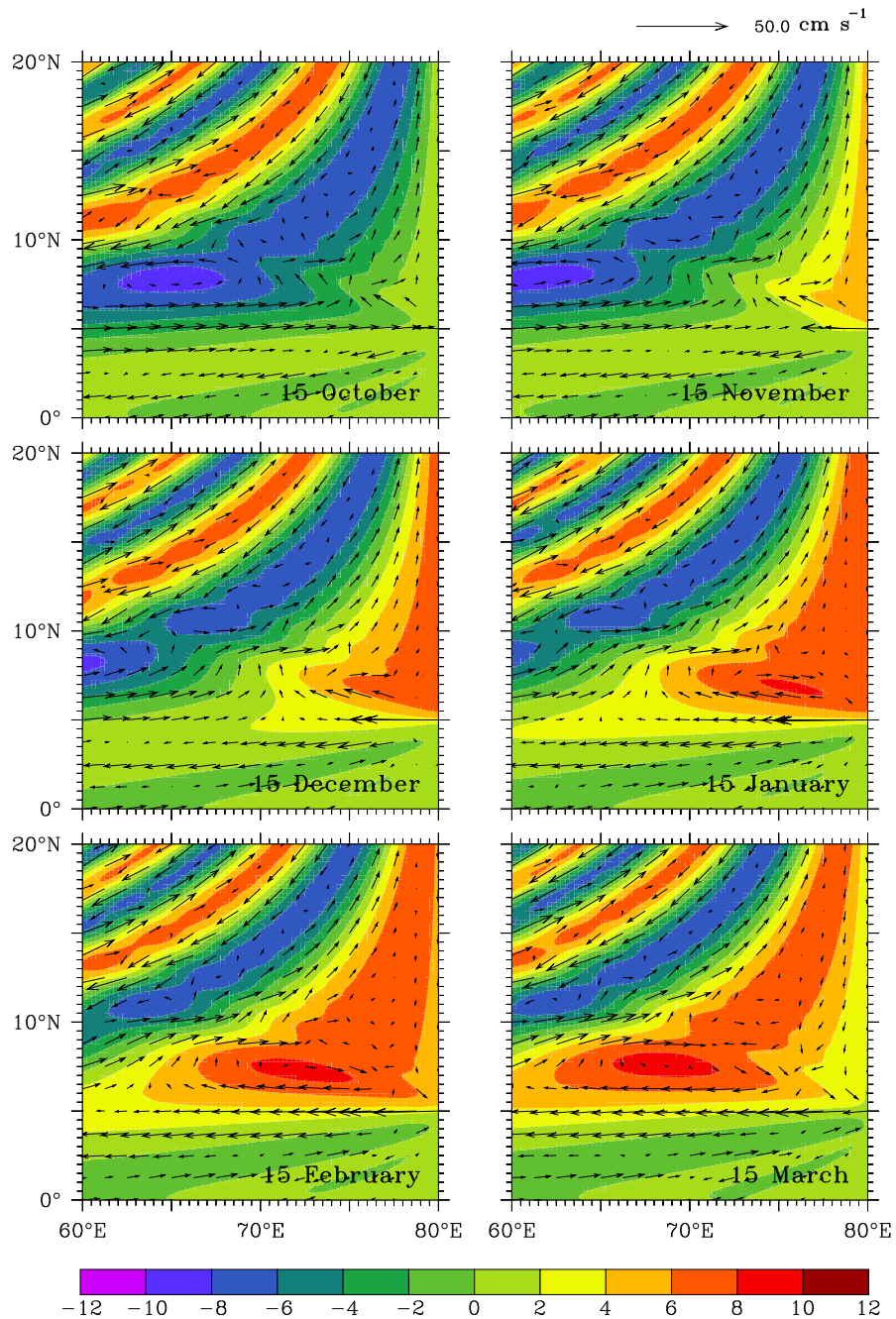


Figure 3.11 Analytic solution for $T = 60$ days; time $t = 0$ and 30 (1 January and 1 February). Sea-level deviation η (cm) and velocity \mathbf{v} (cm s^{-1}) are plotted. A series of highs and lows form at the eastern boundary and propagate westward as Rossby waves; the waves are trapped at the coast north of 7°N .

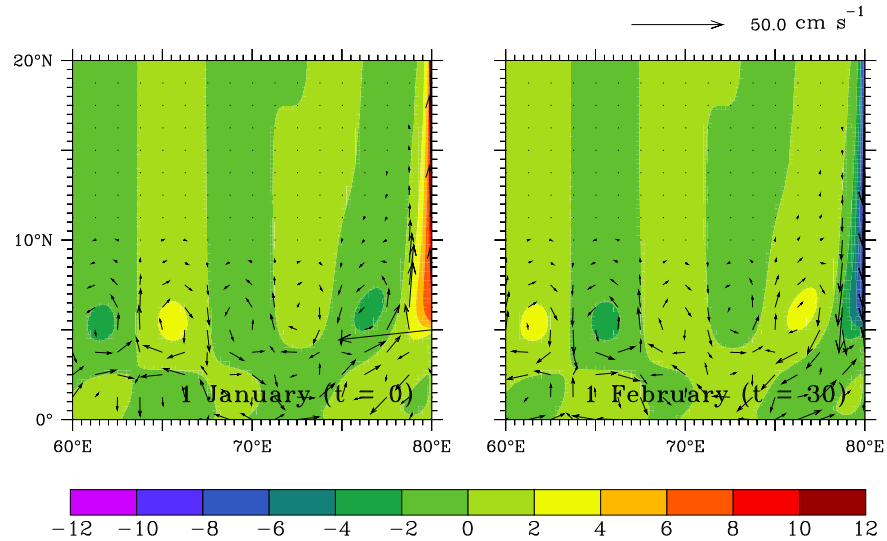
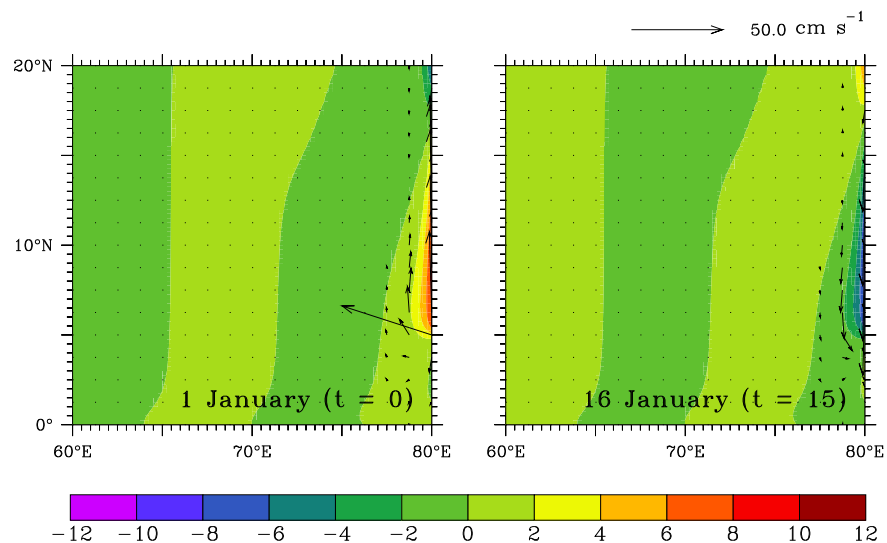


Figure 3.12 Analytic solution for $T = 30$ days; time $t = 0$ and 15 (1 and 16 January). Sea-level deviation η (cm) and velocity \mathbf{v} (cm s^{-1}) are plotted. For a period of 30 days, the critical latitude is 3.5° , to the south of the axis of the zonal current at the eastern boundary. Therefore, Rossby wave radiation is impossible and the high and low do not form.



of the basin, and the latter is close to it. Hence, both annual and semiannual Kelvin waves are inseparable from westward propagating Rossby waves in the Bay of Bengal and the Arabian Sea, and energy leaks at these periods from the eastern boundary into the open ocean¹².

3.5 Forcing Mechanisms

The leaky waveguide in the north Indian Ocean makes the Kelvin wave off the east coast of India more complex than the one discussed in Section 3.4; it is the result of Kelvin waves of different frequencies and phases forced by several mechanisms. McCreary et al. [1996] identified three such mechanisms: local alongshore winds (LA) adjacent to the east coasts of India and Sri Lanka, remote alongshore winds (RA) adjacent to the eastern and northern boundaries of the bay [McCreary et al., 1993], and remote forcing from the equatorial waveguide (EQ) [Potemra et al., 1991; Yu et al., 1991]. The resultant Kelvin wave, on reaching the west coast of India, is modified by the local alongshore winds there (WLA), and the Rossby waves radiated from the coast are modified by Ekman pumping [Bruce et al., 1994, 1998]. In addition, the interaction of equatorial Rossby waves with the southern tip of India can also force Kelvin waves along the Indian west coast [Bruce et al., 1998]. All these processes contribute to the formation of the Lakshadweep high and low.

To isolate the effect of the processes on the Lakshadweep high and low and the WICC, two sets of boundary conditions are applied along continental boundaries [Shankar et al., 1996; McCreary et al., 1996]. One set is the usual no-slip condition

$$u = v = 0. \quad (3.12a)$$

The other set,

$$\tilde{u} = \mathbf{n} \cdot \mathbf{v} = -\mathbf{n} \cdot \mathbf{k} \times \frac{\boldsymbol{\tau}}{f}, \quad \tilde{v} = \mathbf{k} \times \mathbf{n} \cdot \mathbf{v}, \quad (3.12b)$$

is applied to the boundaries of the Bay of Bengal and the west coast of India and Sri Lanka in three of the test solutions. In (3.12b), \mathbf{k} is a unit vector directed out of the β -plane and \mathbf{n} is a unit vector normal to the boundary that points into the bay (offshore) along its western and northern margins, out of the bay (inshore) along its northeastern and eastern margins, and out of the sea (inshore) along the southern boundaries of India and Sri Lanka and along their west coast; $\mathbf{v} = (\tilde{u}, \tilde{v})$, where \tilde{u} and \tilde{v} are the velocity components normal to and along the boundary; and $\boldsymbol{\tau} = (\tau^x, \tau^y)$ is the wind stress. Conditions (3.12b) allow Ekman flows to pass through boundaries, and therefore circulations driven by coastal Ekman pumping are filtered out of the solutions.

¹²See Appendix B, Figure B.2.

The solutions for the processes LA, RA, and WLA are found analogous to McCreary et al. [1996]. The main, or control, run is the linear solution described in Section 3.3.3 (Figure 3.7), for which the condition (3.12a) is applied at continental boundaries. The modifications made to obtain the process solutions are described below.

3.5.1 Winds Along the East Coast of India and Sri Lanka (Process LA)

To isolate the effect of the strong winds that blow along the east coast of India and Sri Lanka, we apply conditions (3.12b) along this coast (from 87°E , 20°N to 82°E , 6.5°N), thereby eliminating the effect of the alongshore winds there. The difference between the main run and this run gives the process solution forced by LA (Figure 3.13).

The winds along the east coast are southwesterly during the southwest monsoon and northeasterly during the northeast monsoon. The southwest–northeast alignment of the coast makes the wind vector virtually parallel to the coast and these winds generate strong Kelvin waves; the EICC closely follows the wind field. Northeasterly winds, which force coastal downwelling, set in with the withdrawal of the southwest monsoon and the EICC reverses to flow equatorward. The Kelvin wave that forces this downwelling EICC also forces a downwelling WICC in November. The subsequent radiation of Rossby waves generates a high off southwest India in January, as in the main run, but the high forced by LA is much stronger. The weakening of the northeast monsoon after January forces coastal upwelling along the east coast; the upwelling intensifies with the onset of the southwest monsoon in May. This upwelling Kelvin wave generates a low off southwest India, but it is weaker than in the main run. Thus, the winds along the western boundary of the Bay of Bengal can force both the high and the low. These winds have a stronger impact on the WICC than they have on the EICC; by themselves, they cannot force the seasonal cycle of the EICC, but they can force the seasonal cycle of circulation off southwest India.

3.5.2 Winds Along the Eastern and Northern Boundaries of the Bay of Bengal (Process RA)

To isolate the effect of the winds that blow along the eastern and northern boundaries of the Bay of Bengal, we apply conditions (3.12b) along these coasts (from 97°E , 2.5°N to 87°E , 20°N), thereby eliminating the effect of the alongshore winds there. The difference between the main run and this run gives the process solution forced by RA (Figure 3.14).

These winds also force Kelvin waves, which propagate along the rim of the bay, radiating Rossby waves from the eastern boundary in the process. The Kelvin waves forced by these winds make a weak contribution to the EICC, forcing coastal upwelling during February–September and downwelling during October–January. Their effect on the high and low is also weak. Though

Figure 3.13 Effect of winds along the east coast of India and Sri Lanka (Process LA). Plots of sea-level deviation η (cm) and velocity \mathbf{v} (cm s^{-1}) are shown. Process LA forces a high off southwest India in January; the high propagates westward, as in the main run. The low that formed during the southwest monsoon is also seen in the central Arabian Sea. Its reflection at the coast of Arabia forces an upwelling-favourable current there.

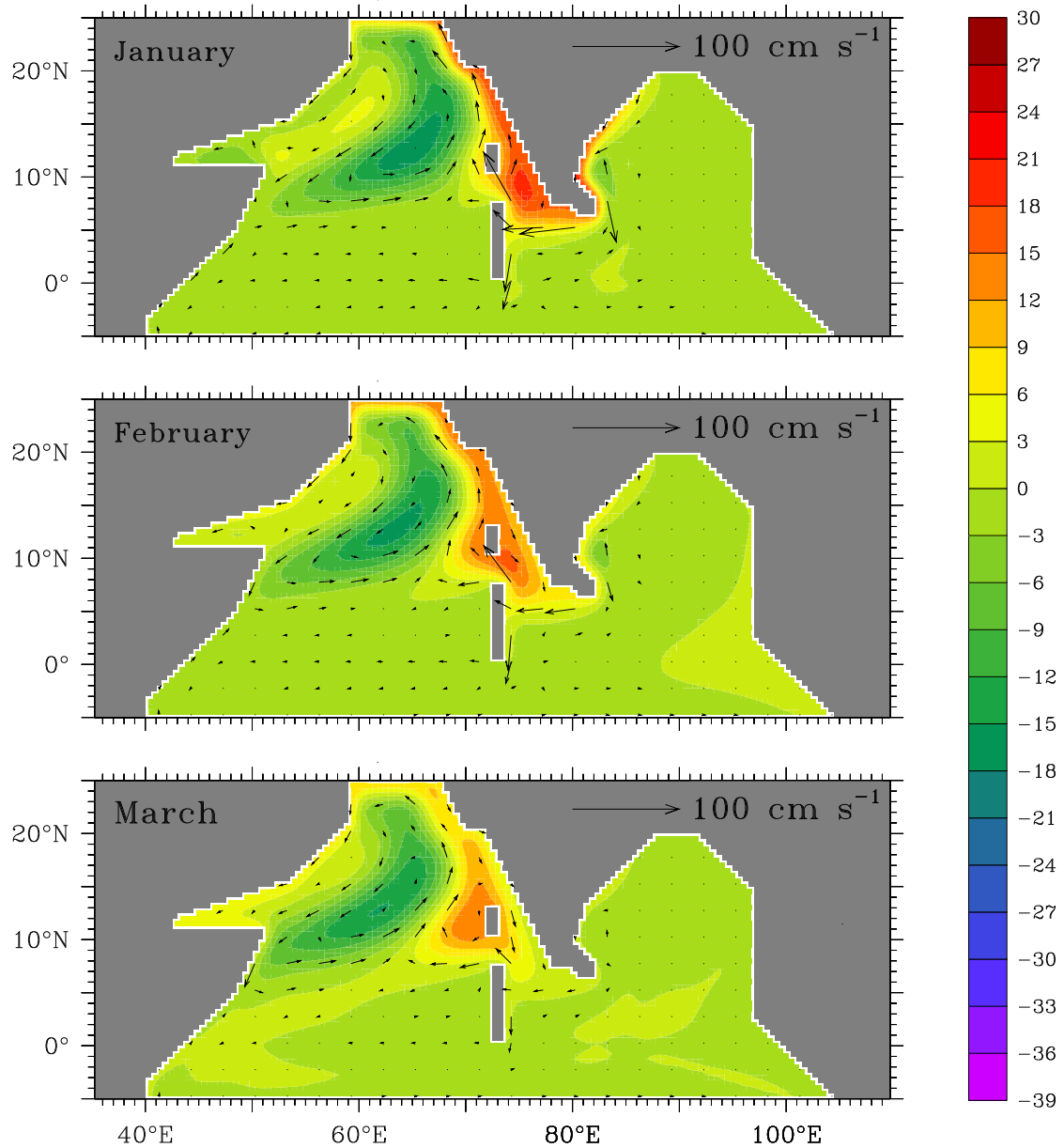


Figure 3.13 (continued) Effect of winds along the east coast of India and Sri Lanka (Process LA). Plots of sea-level deviation η (cm) and velocity \mathbf{v} (cm s^{-1}) are shown. The Lakshadweep high propagates westward; in April, it is located to the west of the Lakshadweep islands. An equatorward WICC forms in May, and by June, the incipient Lakshadweep low is seen off southwest India. The Rossby waves that constitute the Lakshadweep high and low also have an effect on the circulation in the northwestern Arabian Sea.

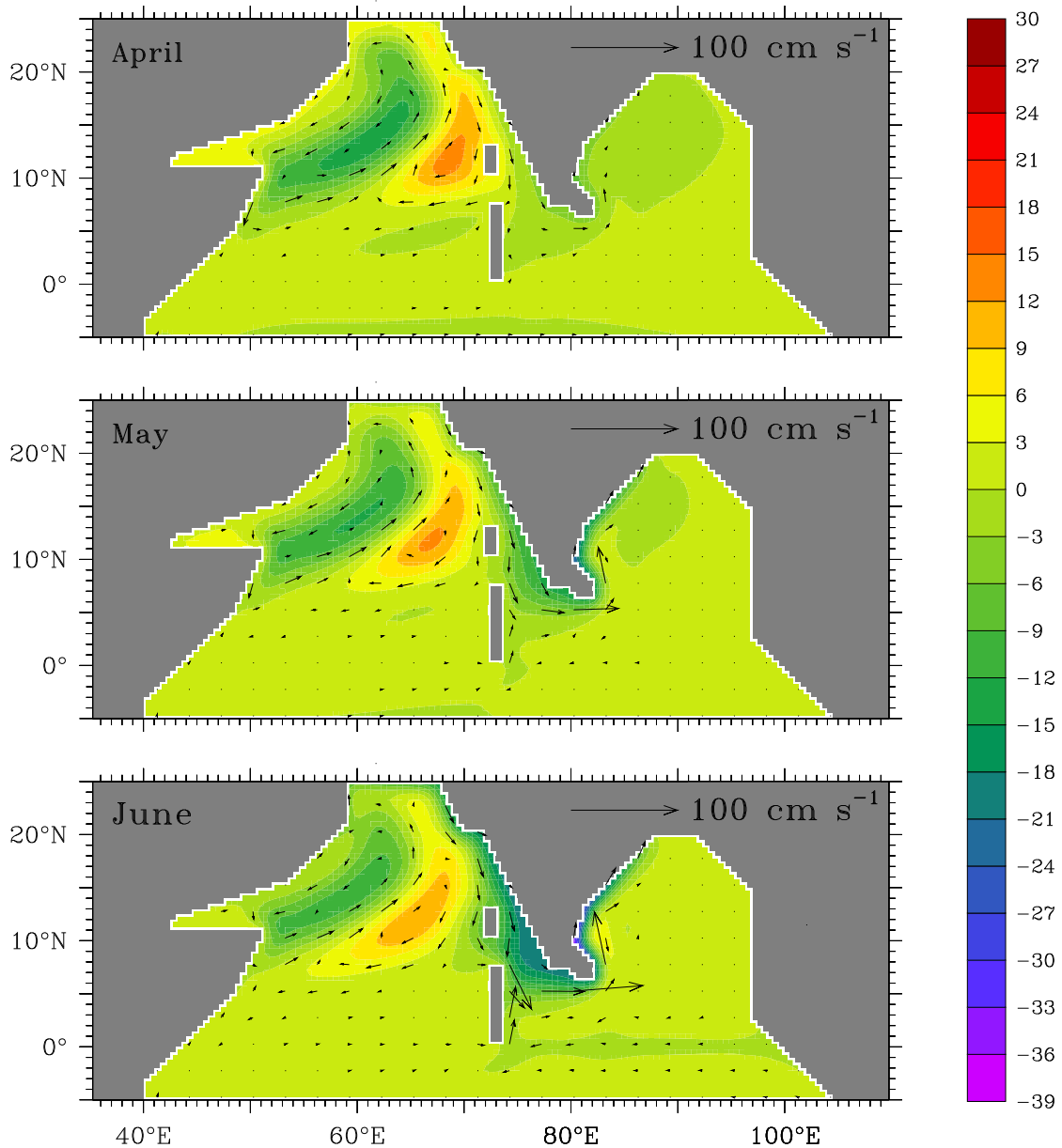


Figure 3.13 (continued) Effect of winds along the east coast of India and Sri Lanka (Process LA). Plots of sea-level deviation η (cm) and velocity \mathbf{v} (cm s^{-1}) are shown. During the southwest monsoon, process LA forces a poleward EICC along the coast of India and Sri Lanka. This current is the continuation of the SMC, whose meandering structure in the Arabian Sea is associated with the Lakshadweep high and low.

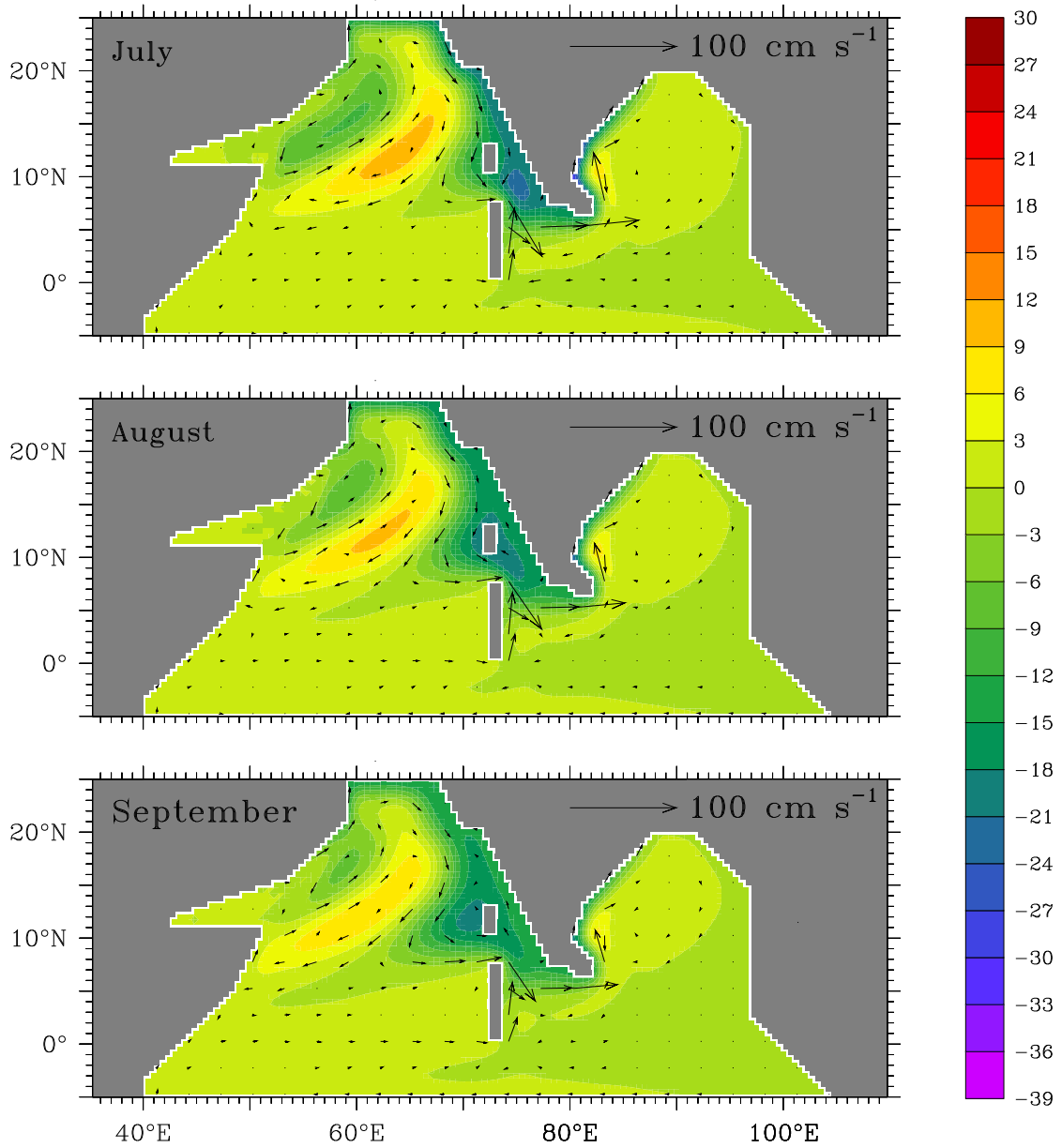


Figure 3.13 (continued) Effect of winds along the east coast of India and Sri Lanka (Process LA). Plots of sea-level deviation η (cm) and velocity \mathbf{v} (cm s^{-1}) are shown. The winds along the east coast of India and Sri Lanka reverse after the collapse of the southwest monsoon, forcing an equatorward EICC. The EICC flows around Sri Lanka into the poleward WICC. By December, the incipient Lakshadweep high is seen off southwest India.

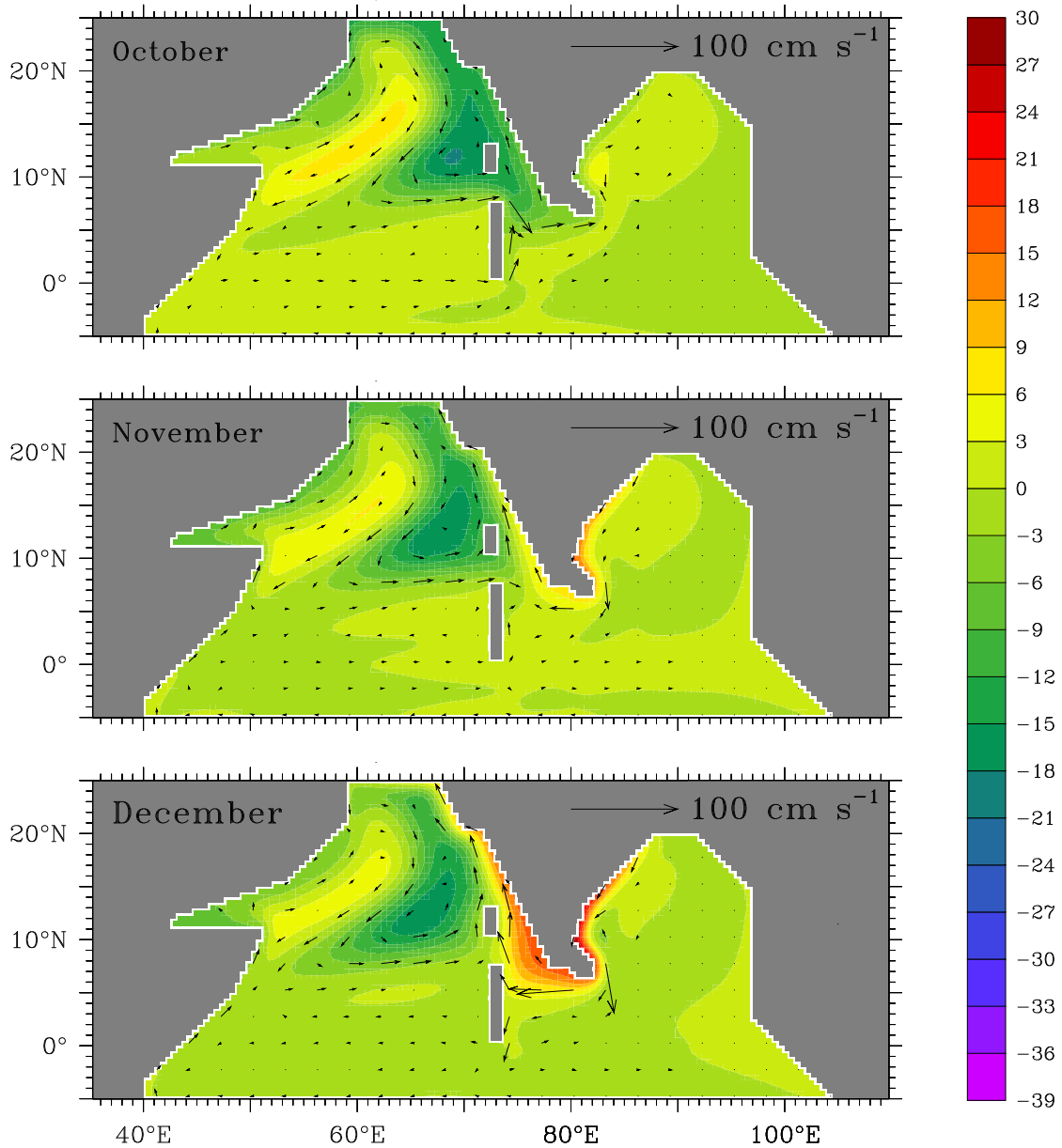


Figure 3.14 Effect of winds along the eastern and northern boundaries of the Bay of Bengal (Process RA). Bimonthly plots of sea-level deviation η (cm) and velocity \mathbf{v} (cm s^{-1}) are shown. Though the winds along the eastern and northern boundaries of the bay are comparable to those along its western boundary, the response to them is weak because these winds blow almost normal to the coast, forcing a weak Kelvin wave.

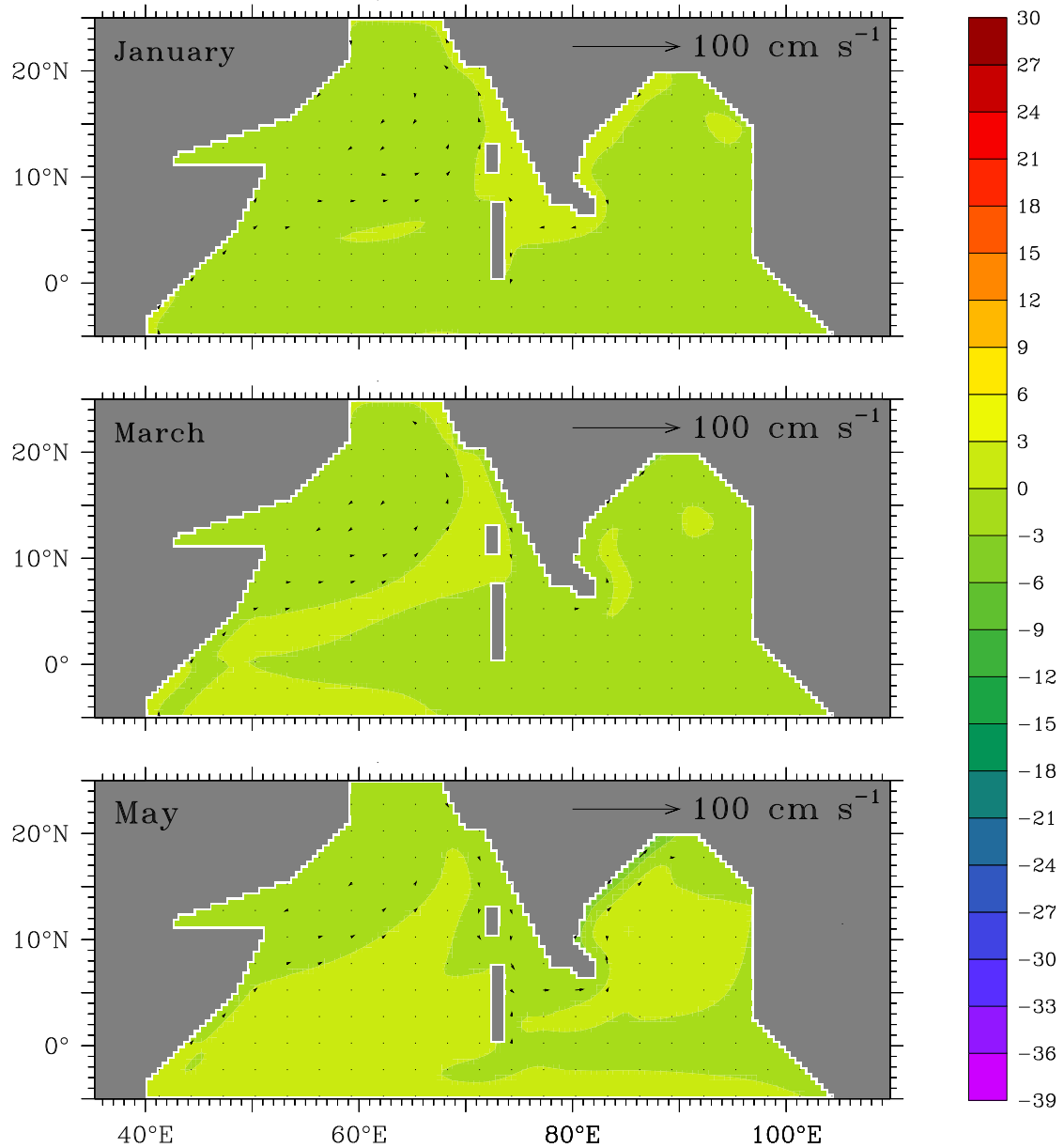
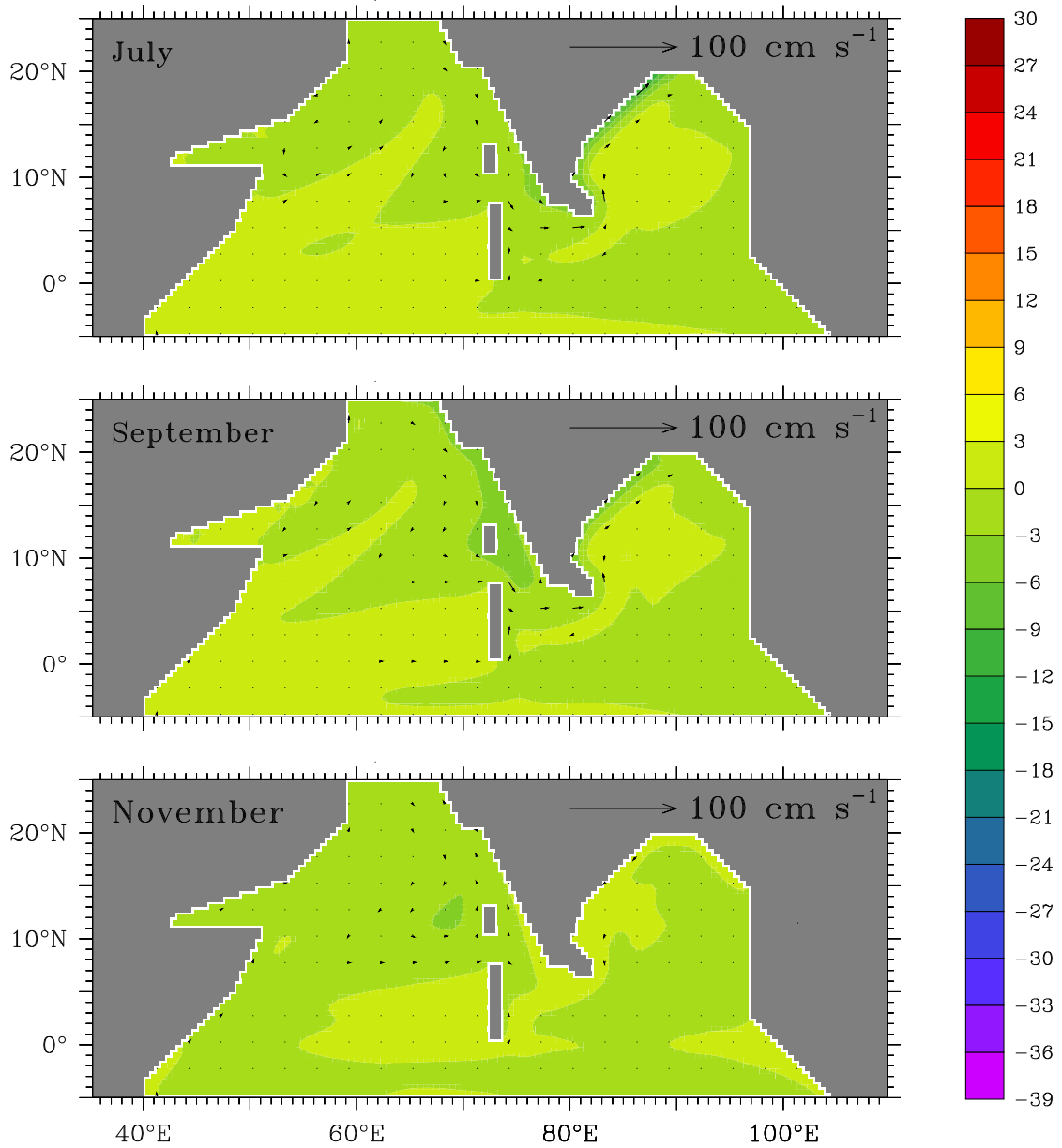


Figure 3.14 (continued) Effect of winds along the eastern and northern boundaries of the Bay of Bengal (Process RA). Bimonthly plots of sea-level deviation η (cm) and velocity \mathbf{v} (cm s^{-1}) are shown. During the southwest monsoon, process RA forces a weak, poleward EICC, complementing process LA; the Kelvin waves that force this EICC also force a weak, equatorward WICC.



the effect of process RA is much weaker than that of LA, the winds in the eastern bay are not significantly weaker than those in the western bay; it is the alignment of the coast, almost normal to the wind vector, that results in a weak alongshore component, and hence, in a weak response.

3.5.3 Winds Along the West Coast of Sri Lanka and India (Process WLA)

To isolate the effect of the winds that blow along the west coast of Sri Lanka and India, we apply conditions (3.12b) along this coast (from 82°E , 6.5°N to 67.5°E , 25°N), thereby eliminating the effect of the alongshore winds there. The difference between the main run and this run gives the process solution forced by WLA (Figure 3.15).

Along this coast, the winds blow equatorward throughout the year, the winds along the west coast of Sri Lanka being the exception; here, the winds are similar to those along the Indian east coast. During the southwest monsoon, the southwesterlies over the Arabian Sea turn around in the central Arabian Sea to blow from the northwest along the Indian west coast. These winds favour coastal upwelling and are stronger than the equatorward winds during the northeast monsoon. The alignment of the coast also ensures that the winds during the northeast monsoon generate but a weak Kelvin wave. Therefore, though the winds along the eastern boundary of the Arabian Sea do not contribute significantly to the high, they force a low off southwest India and drive the strong upwelling off western and northwestern India during the southwest monsoon.

3.5.4 Other Processes (Processes OP)

The three process solutions described above show that Kelvin waves forced by winds blowing along the east and west coasts of India and Sri Lanka can force the Lakshadweep high and low. To examine the contribution of other processes, we apply conditions (3.12b) from (97°E , 2.5°N) to (67.5°E , 25°N), filtering out processes LA, RA, and WLA. The resulting model response is due to all other processes; these include equatorial Kelvin and Rossby waves, Ekman pumping in the Lakshadweep Sea, and the interaction of equatorial Rossby waves with the southern tip of India (Figure 3.16). The difference between the main run and this run gives the combined effect of LA, RA, and WLA (Figure 3.17).

When the effect of the winds along the coasts of India and Sri Lanka is filtered out of the response, the most striking discrepancies occur in the eastern and northern Arabian Sea. The other processes force but a weak “high” off southwest India. The low does not form during the southwest monsoon, downwelling occurring along most of the west coast instead. This distorts the circulation in the eastern, central, and northern Arabian Sea, with the SMC virtually disappearing to the west of Sri Lanka. This implies that the curious meandering structure of the SMC in the central Arabian Sea is a consequence of the Lakshadweep high and low and is forced by the winds along the coasts of India and Sri Lanka (Figure 3.17). To the east of Sri Lanka, however, the SMC

Figure 3.15 Effect of winds along the west coast of Sri Lanka and India (Process WLA). Plots of sea-level deviation η (cm) and velocity \mathbf{v} (cm s^{-1}) are shown. The winds during the northeast monsoon blow normal to the west coast of India and force a weak Kelvin wave; hence, process WLA forces a weak high off southwest India. It has a stronger effect on the low, and the reflection of the low at the coast of Arabia forces an upwelling-favourable current there throughout the year.

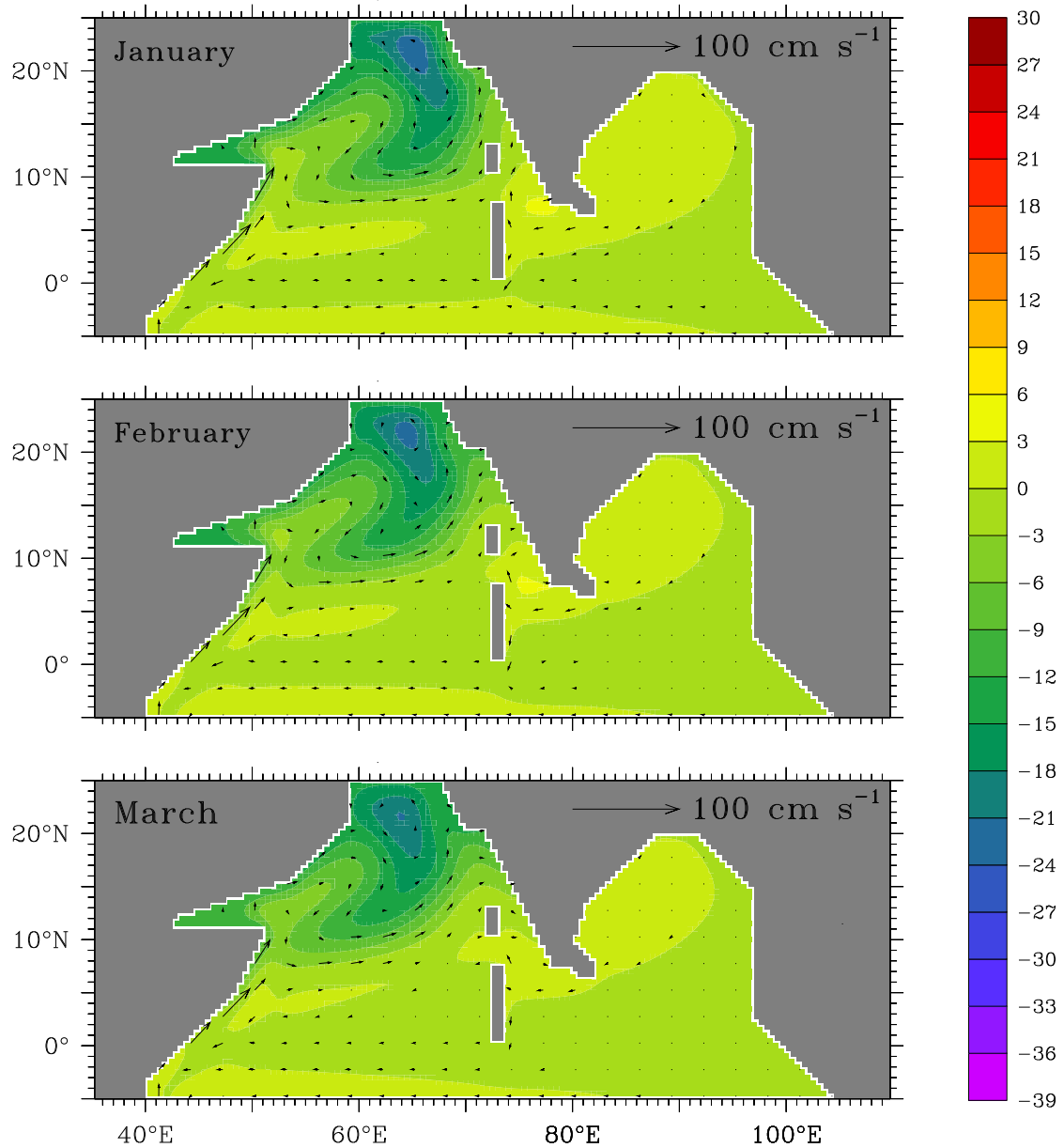


Figure 3.15 (continued) Effect of winds along the west coast of Sri Lanka and India (Process WLA). Plots of sea-level deviation η (cm) and velocity \mathbf{v} (cm s^{-1}) are shown. The effect of the low forced by process WLA and its reflection at the western boundary of the Arabian Sea is felt even in April and May, when process WLA forces a poleward current along the coast of Somalia. This current forces upwelling in the northern part of the Somali coast even before the onset of the southwest monsoon.

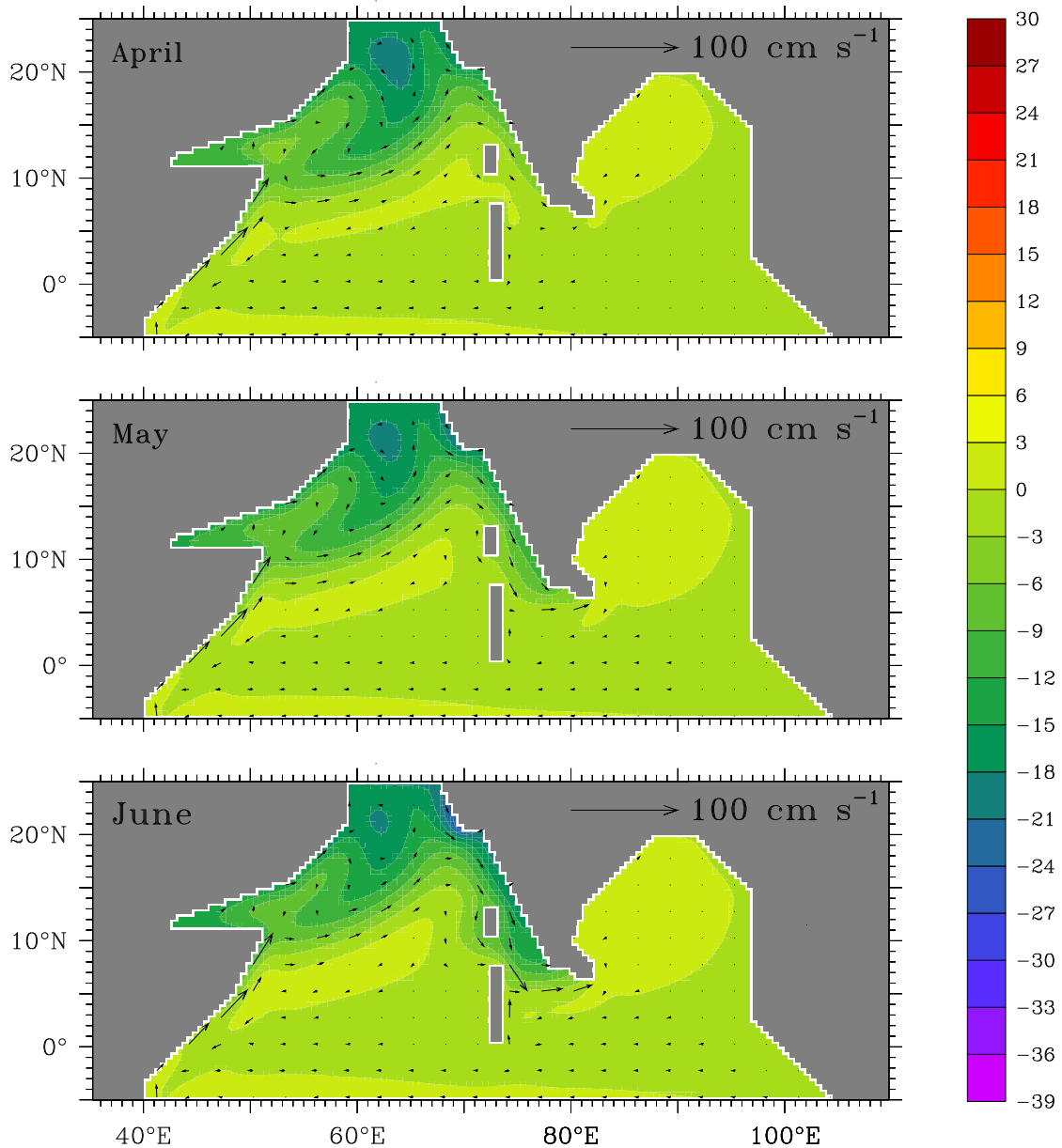


Figure 3.15 (continued) Effect of winds along the west coast of Sri Lanka and India (Process WLA). Plots of sea-level deviation η (cm) and velocity v (cm s^{-1}) are shown. The winds along the west coast of India and Sri Lanka force a low off southwest India by July. The WICC flows equatorward into the SMC. Though process WLA, like LA, can force the SMC, the relatively weak high forced during the northeast monsoon weakens the SMC in the central Arabian Sea.

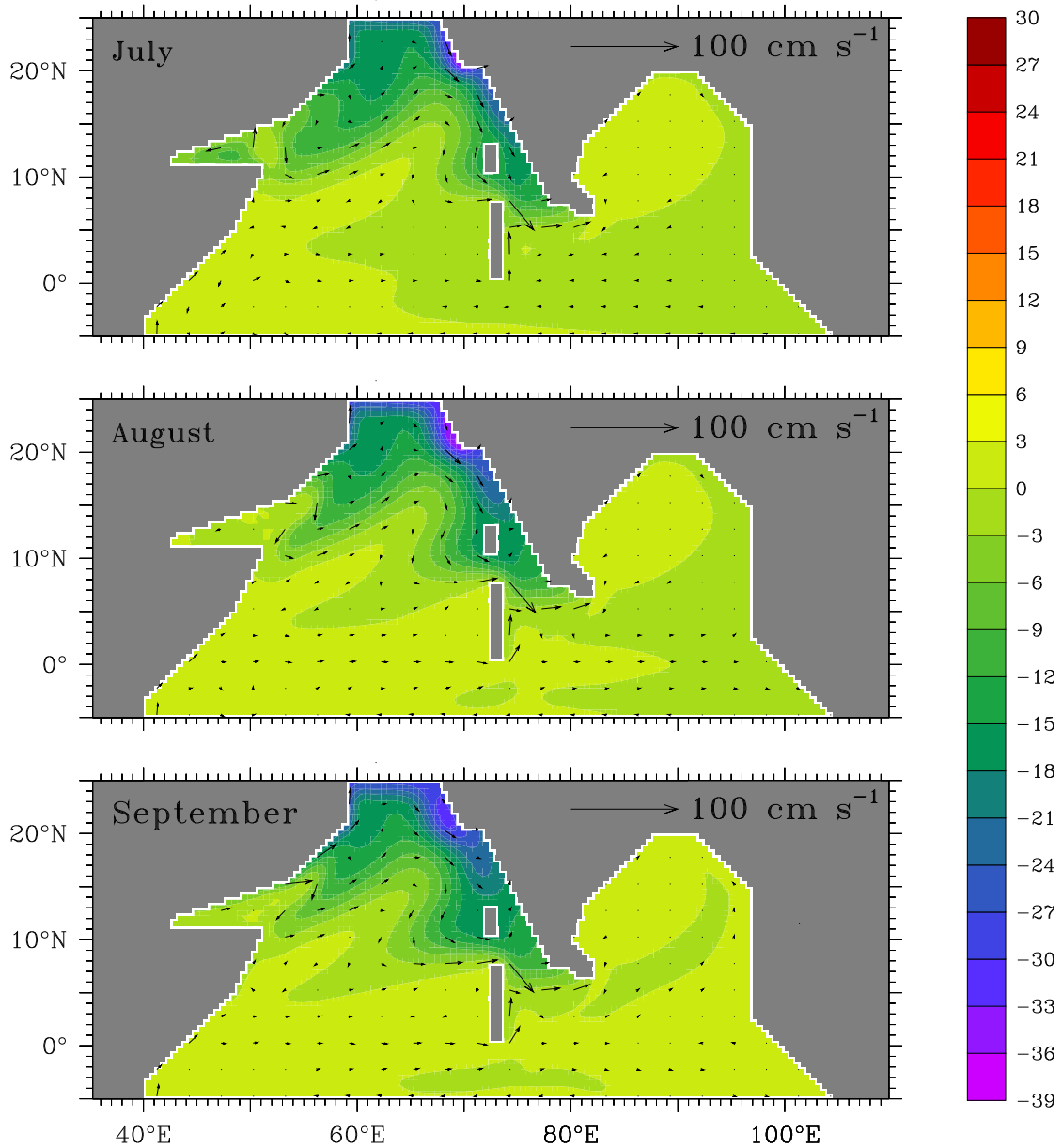


Figure 3.15 (continued) Effect of winds along the west coast of Sri Lanka and India (Process WLA). Plots of sea-level deviation η (cm) and velocity \mathbf{v} (cm s^{-1}) are shown. By October, the low is located to the west of the Lakshadweep islands. The upwelling Kelvin wave forced by process WLA during the southwest monsoon propagates along the rim of the Arabian Sea, forcing upwelling off Arabia and Somalia in winter, opposing the downwelling forced by the local winds.

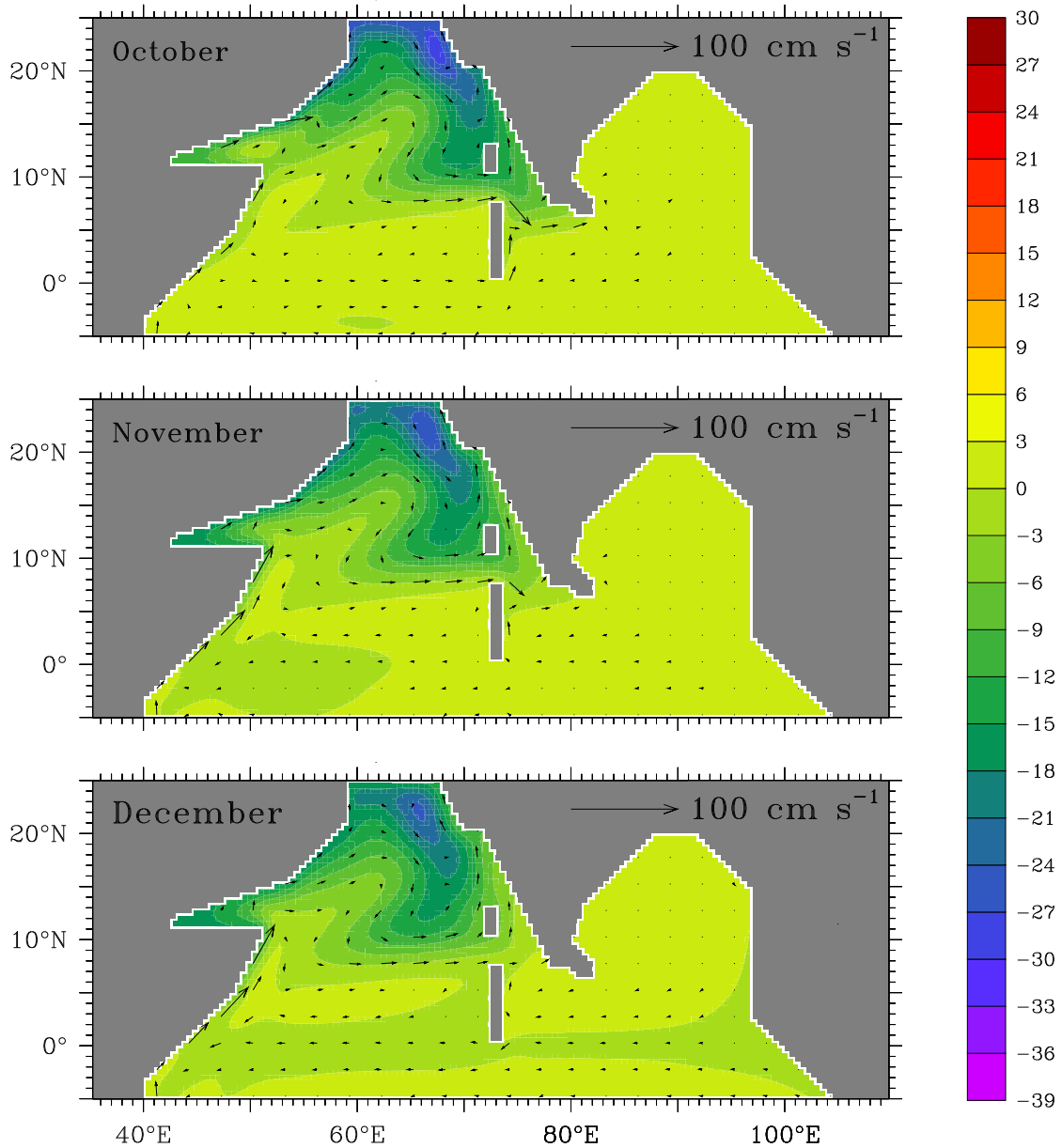


Figure 3.16 Effect of other processes (Processes OP). The effect of processes LA, WLA, and RA has been filtered out of the response. Plots of sea-level deviation η (cm) and velocity \mathbf{v} (cm s^{-1}) are shown. Eliminating the Kelvin waves forced by the alongshore winds in the Bay of Bengal and the eastern Arabian Sea weakens the high off southwest India. Instead, a stronger anticyclonic circulation, with a high in sea level, is seen in the northern Arabian Sea. These processes, however, are responsible for forcing the circulation in the Bay of Bengal throughout the year; the only exception is the EICC, which is also affected by process LA.

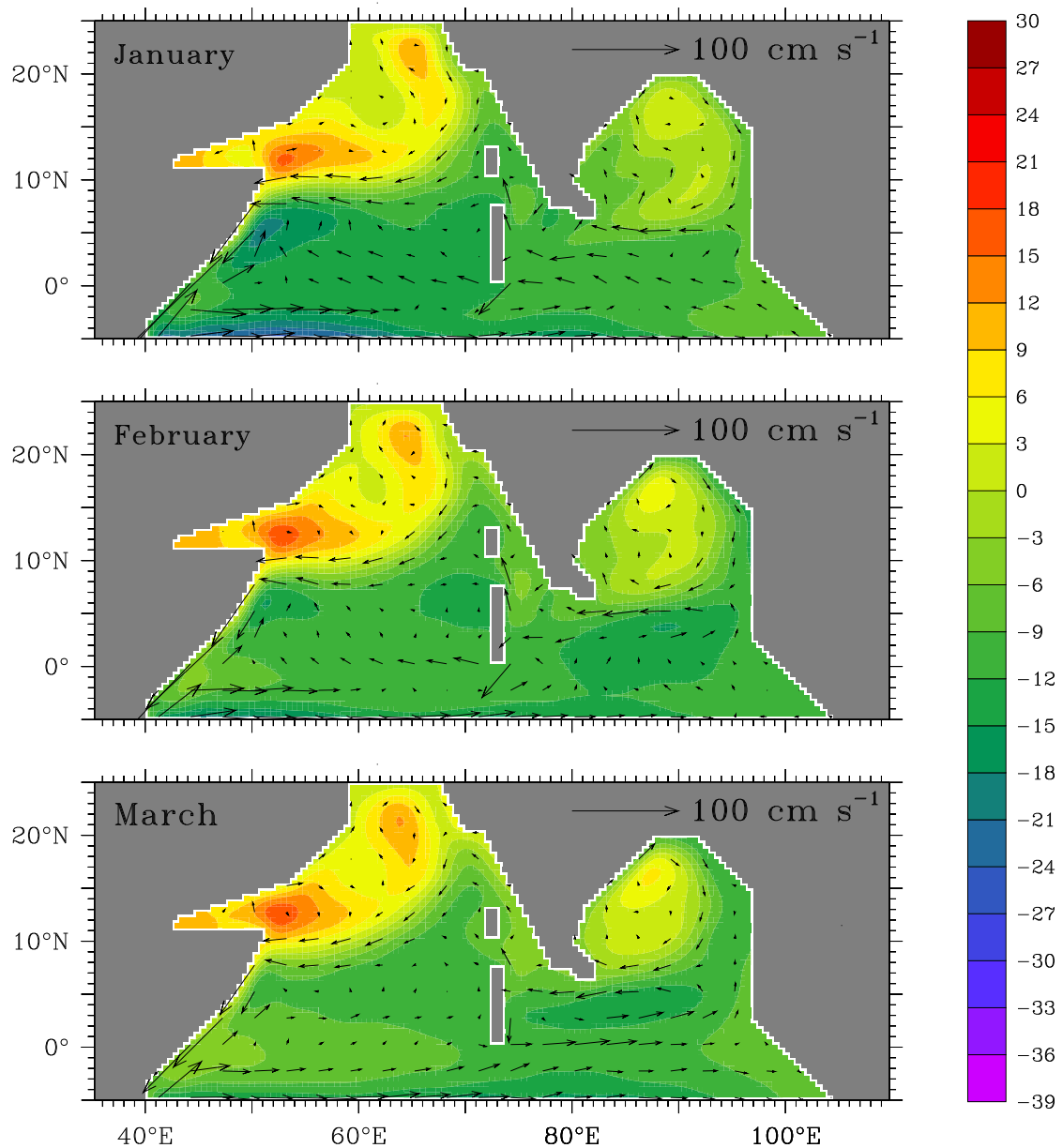


Figure 3.16 (continued) Effect of other processes (OP). The effect of processes LA, WLA, and RA has been filtered out of the response. Plots of sea-level deviation η (cm) and velocity \mathbf{v} (cm s^{-1}) are shown. The absence of the alongshore winds is felt most strongly in the eastern, central, and northern Arabian Sea. The NMC does not weaken in the Arabian Sea and the eastward SMC is restricted to the east of Sri Lanka. The upwelling current off Arabia is weaker than in the main run and the EICC flows equatorward during the southwest monsoon because of Ekman pumping in the interior bay and remote forcing from the equator [Shankar et al., 1996; McCreary et al., 1996].

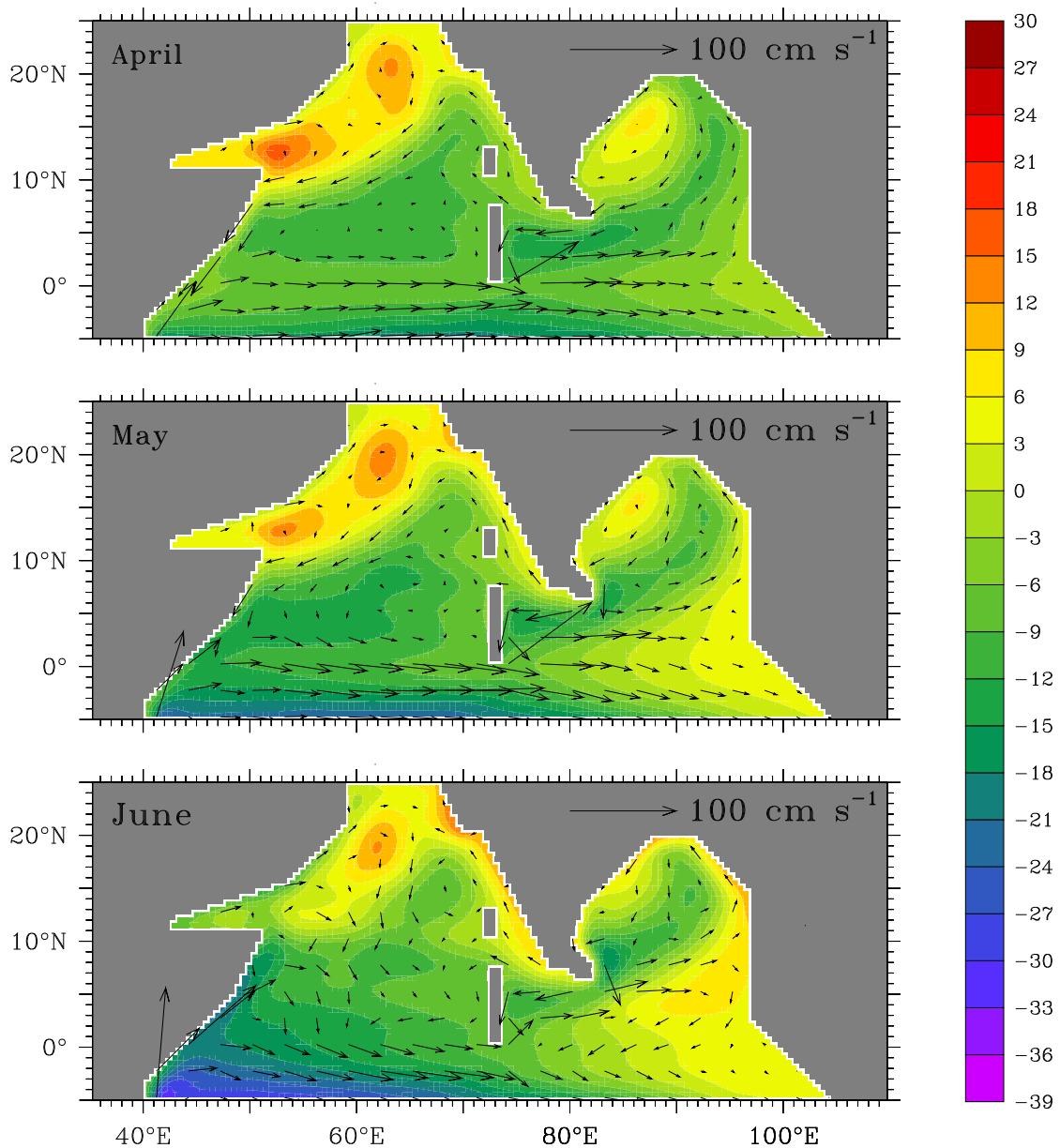


Figure 3.16 (continued) Effect of other processes (Processes OP). The effect of processes LA, WLA, and RA has been filtered out of the response. Plots of sea-level deviation η (cm) and velocity \mathbf{v} (cm s^{-1}) are shown. Processes OP force a westward “SMC” to the west of Sri Lanka. This current flows through the gap between the Lakshadweep and Maldive islands and joins the return flow around the anticyclonic highs in the western Arabian Sea. Processes OP, however, are the principal causes of the circulation in the western Arabian Sea.

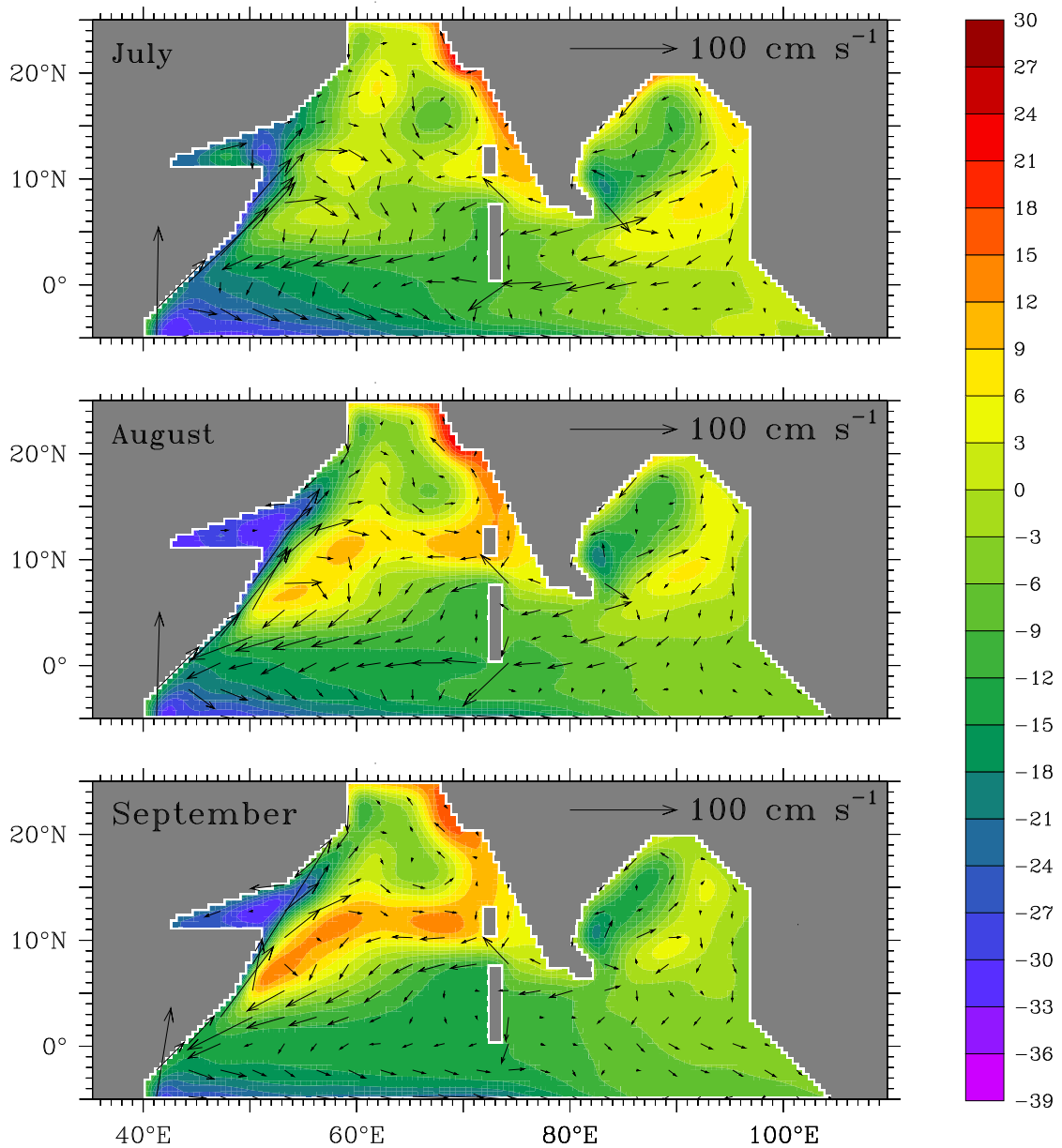


Figure 3.16 (continued) Effect of other processes (Processes OP). The effect of processes LA, WLA, and RA have been filtered out of the response. Plots of sea-level deviation η (cm) and velocity \mathbf{v} (cm s^{-1}) are shown. The major distortion during October–December occurs in the Arabian Sea and off the east coast of Sri Lanka, where a weak EICC flows poleward in the absence of local winds. In the northern and central Arabian Sea, the absence of a low during the southwest monsoon results in a high in sea level. In the rest of the basin, however, it is the processes OP that determine the circulation.

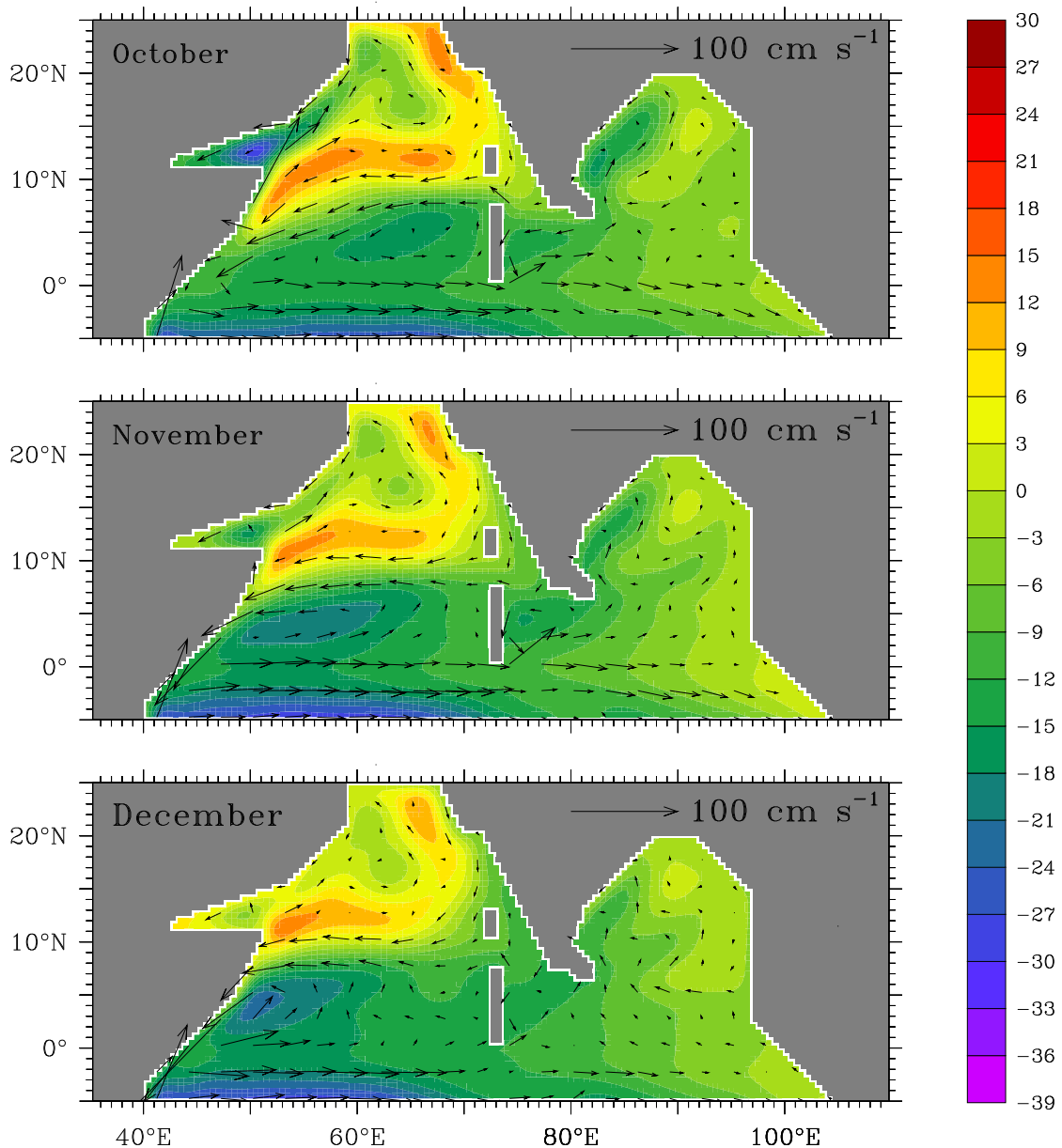


Figure 3.17 Effect of processes LA, RA, and WLA. Only these three processes are retained in this solution. Plots of sea-level deviation η (cm) and velocity \mathbf{v} (cm s^{-1}) are shown. The winds blowing along the coasts of India and Sri Lanka are the principal causes of the circulation in the eastern, central, and northern Arabian Sea. Elsewhere, except for the effect of process LA on the EICC, their impact is small.

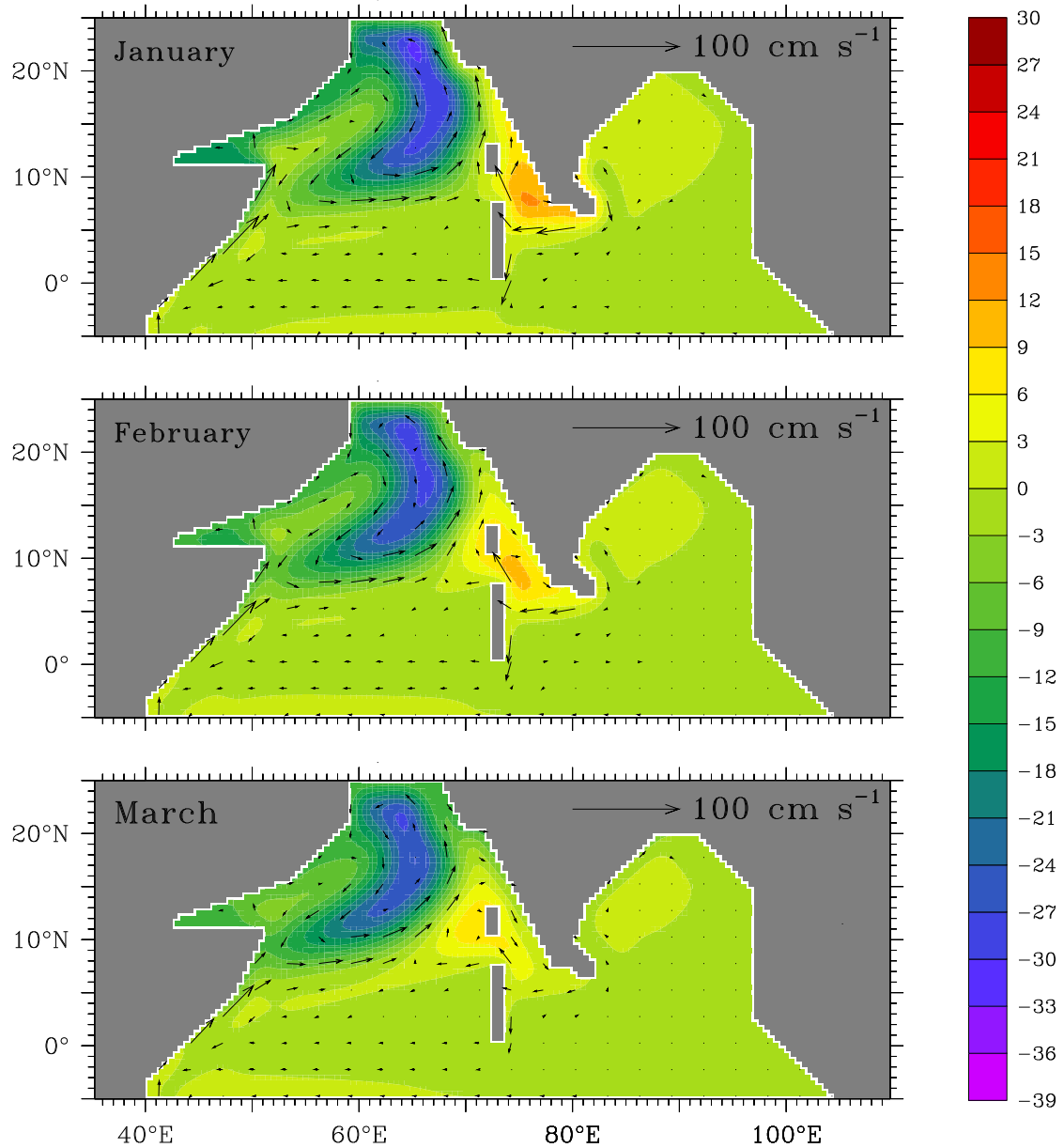


Figure 3.17 (continued) Effect of processes LA, RA, and WLA. Only these three processes are retained in this solution. Plots of sea-level deviation η (cm) and velocity \mathbf{v} (cm s^{-1}) are shown. The Lakshadweep high is forced principally by process LA, with smaller contributions from WLA and OP. The high stretches westward across the southern Arabian Sea by May; its slower propagation in the main run is because of processes OP.

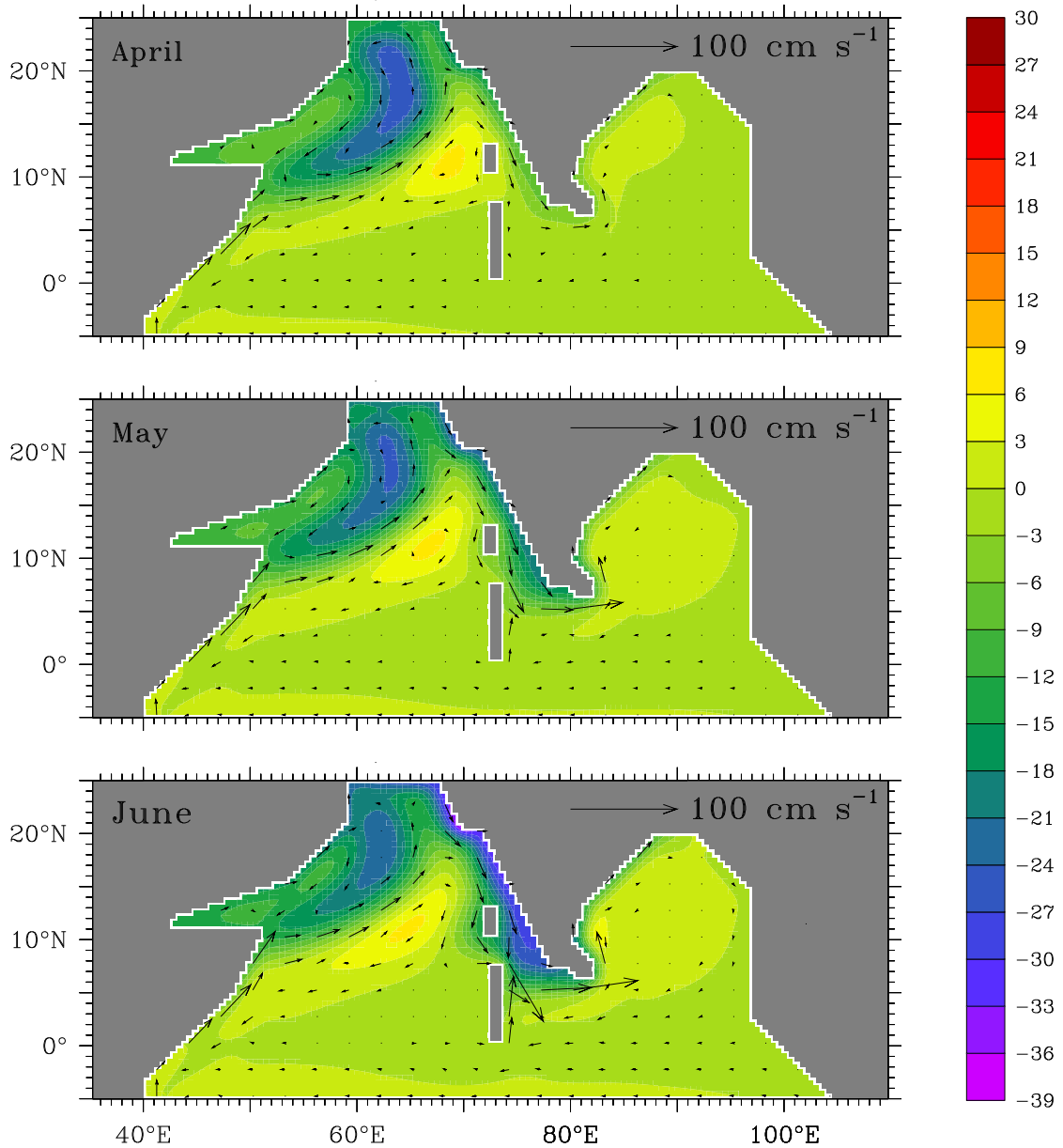


Figure 3.17 (continued) Effect of processes LA, RA, and WLA. Only these three processes are retained in this solution. Plots of sea-level deviation η (cm) and velocity \mathbf{v} (cm s^{-1}) are shown. Processes WLA and LA force strong upwelling off the west coast of India and Sri Lanka during the southwest monsoon. The upwelling signal propagates as a Kelvin wave and complements the local winds that force upwelling off Arabia. The SMC to the west of Sri Lanka is forced by processes LA and WLA; other processes (OP) force a westward current and weaken the SMC forced by LA and WLA. These other processes, however, are the cause of the SMC to the east of Sri Lanka [Vinayachandran and Yamagata, 1998].

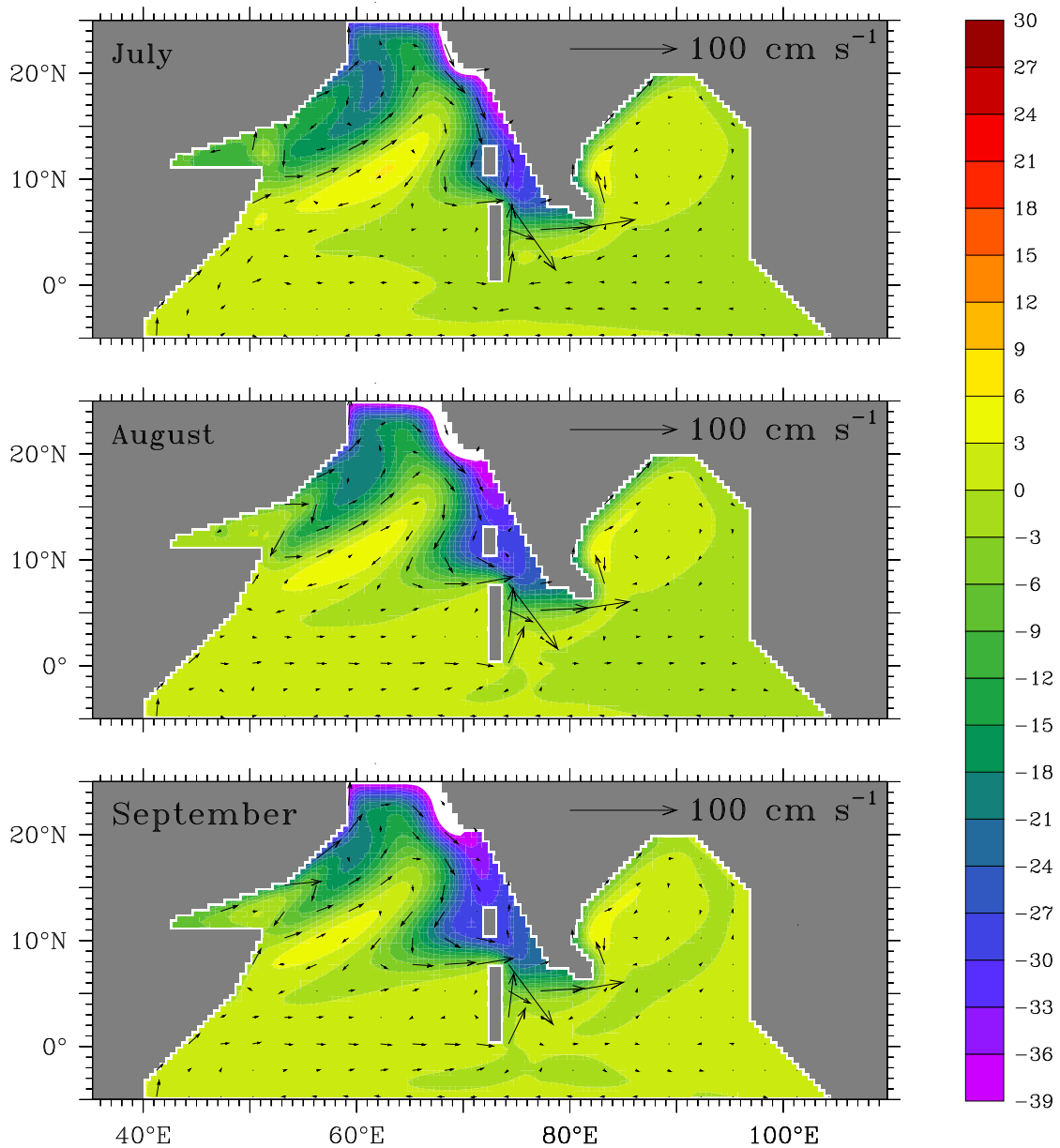
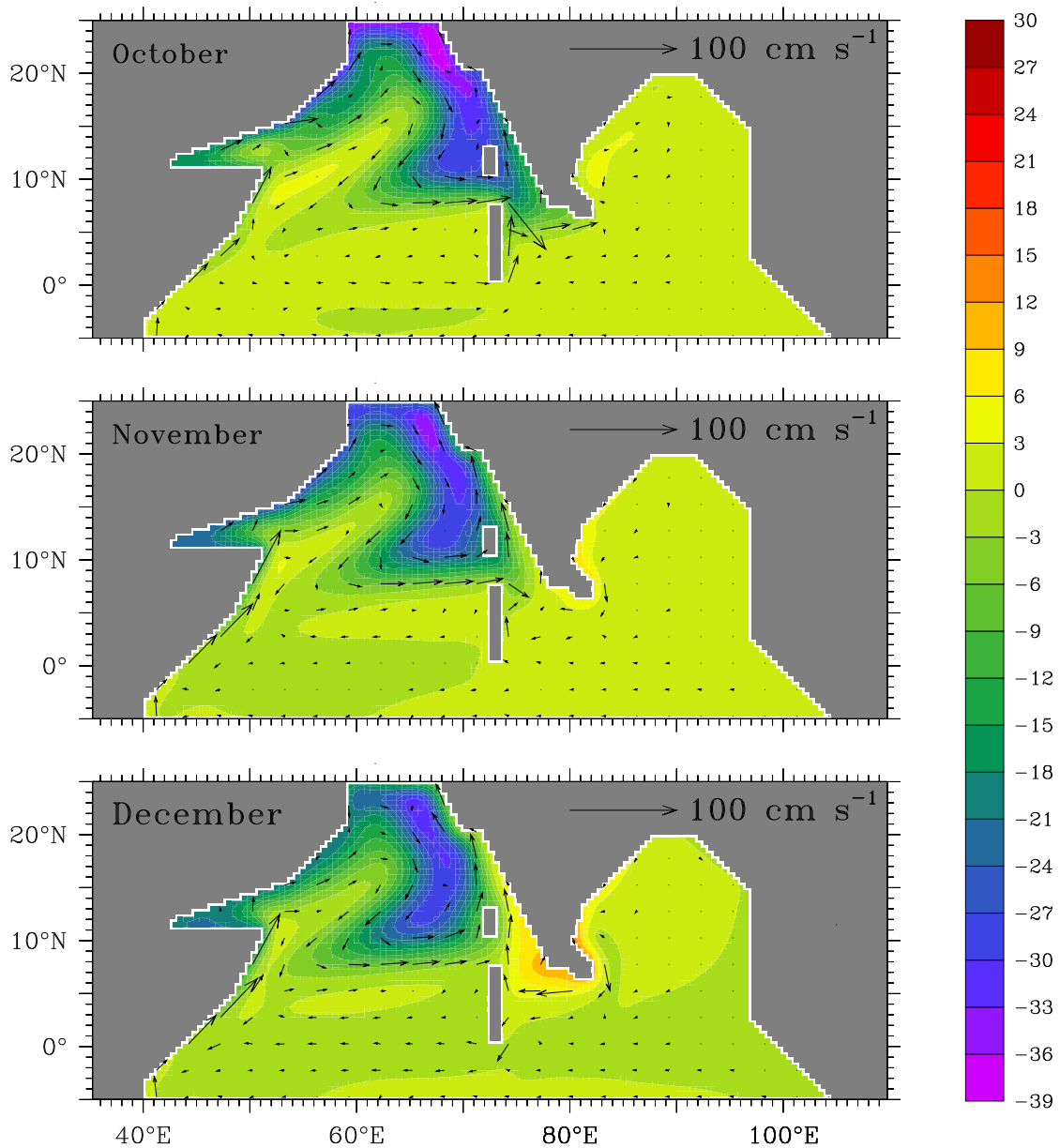


Figure 3.17 (continued) Effect of processes LA, RA, and WLA. Only these three processes are retained in this solution. Plots of sea-level deviation η (cm) and velocity \mathbf{v} (cm s^{-1}) are shown. The low forced by processes LA and WLA propagates westward during October–December and an incipient high forms off southwest India in December. The absence of the local winds off Somalia and the forcing from the equator weakens the flow along the western flank of the low. This flow is enhanced in the main run by the formation of the Great Whirl and the Socotra high; the westward propagation of the Lakshadweep high, which is forced mainly by LA, makes a minor contribution to these highs in September and October.



is forced by the equatorial waves and Ekman pumping in the interior bay [Vinayachandran and Yamagata, 1998]. The result of processes OP is a bizarre SMC: it is eastward to the east of Sri Lanka, westward to its west.

These process solutions show that the winds along the coasts of India and Sri Lanka have a strong effect on the circulation in the Arabian Sea; in the Bay of Bengal, their effect is restricted to the east coast of India and Sri Lanka. These winds are the principal mechanisms responsible for the Lakshadweep high and low and the seasonal cycle of circulation in the eastern Arabian Sea. The Kelvin waves forced by these winds also affect the Somali current, but not to the same magnitude. They force an upwelling current off Somalia almost throughout the year, weakening the equatorward Somali current in its northern reaches before the dramatic effect of the equatorial waves and local winds can be felt there with the onset of the southwest monsoon.

Thus, the effect of the processes that lead to the Lakshadweep high and low can be felt over large parts of the Arabian Sea. Since they are forced by the monsoon winds that blow year after year, the high and low must form year after year, and the variability associated with the monsoon must force variations in the high and low over a range of time scales. Such a strong seasonal cycle in the ocean and the variability associated with it must have some effect beyond modifying the circulation of the upper ocean in the region. We conclude this chapter with a brief discussion on some implications of the Lakshadweep high and low.

3.6 Implications of the Lakshadweep High and Low

The Lakshadweep high raises sea level and lowers the pycnocline in the Lakshadweep Sea during January to April. This implies a thick, stable upper layer that can warm more easily. This stability is enhanced by low-salinity water from the Bay of Bengal, brought in by the equatorward EICC and the NMC. Shenoi et al. [1999] argue that the high sea-surface temperatures (SSTs) that occur there as early as March, well before the thermal equator moves over the region, and the monsoon onset vortex that forms there later and heralds the onset of the southwest monsoon over India, are intimately connected to the high. Their hypothesis has all the elements of a classical coupled ocean-atmosphere system. First, an atmospheric event well separated from the eventual region of intense activity triggers events in the ocean. (The collapse of the southwest monsoon in October and the onset of the northeast monsoon generate Kelvin waves in the Bay of Bengal.) Second, response entirely within the ocean produces special conditions at a location remote from the atmospheric event. (The Kelvin waves from the bay lead to downwelling and to a stable surface layer off southwest India, resulting in higher SSTs there.) Third, the ocean triggers an event in the atmosphere. (High SSTs lead to the monsoon onset vortex.)

The Lakshadweep high is also important for the fishery of India. Upwelling along this coast be-

gins sometime in February [Longhurst and Wooster, 1990], well before the onset of the upwelling-favourable southwest monsoon winds. As seen in Figures 3.8 and 3.10, a consequence of the remotely forced Kelvin wave is the formation of a weak, but upwelling-favourable coastal current off southwest India, this current being integral to the dynamics of the high. The early upwelling is therefore one manifestation of the process discussed above. This upwelling current strengthens and leads to the low during the southwest monsoon. The result is an intense upwelling regime in the Lakshadweep Sea and farther north along the Indian west coast, with consequences for the marine chemistry of the region. Upwelling brings up the nutrient-rich deeper water, leading to a growth of phytoplankton, and to the depletion of oxygen in the surface waters due to their mixing with the anoxic deeper waters. These changes in the chemistry and primary productivity have an impact on the fishery of the region [Banse, 1968; Naqvi et al., 1998].

Thus, apart from the physical oceanography of the Arabian Sea, the Lakshadweep high and low have cascading effects on the atmosphere above, and on the marine chemistry and biology of the eastern Arabian Sea. The implications of the high and low are still being unravelled and form an area of active research. Our interest is in the variability of sea level along the Indian coast, and, having described the theoretical framework for studying the dynamics of the north Indian Ocean, it is to the seasonal cycle of coastal sea level that we turn our attention. It is obvious that the dynamics associated with the high and low must have a bearing on the seasonal cycle of sea level along the west coast of India. Most significant is the importance of remote forcing, especially of the high, which appears to be forced primarily by the winds blowing along the east coast of India and Sri Lanka. This bears out our tentative conclusion, drawn earlier on the basis of Figure 2.8, that the winds at a location along the Indian coast are not a sufficient cause of the sea-level changes there; the north Indian Ocean must be considered as a whole to model the observed variability. The $1\frac{1}{2}$ -layer reduced-gravity model is successful in simulating the essential features of the circulation in the basin, including the large-scale coastal currents. In the following chapter, we apply it to the study of the seasonal cycle of sea level along the coast of India.